Article

Controlling Electron Transfer between the Two Cofactor Chains of Photosystem I by the Redox State of One of Their Components

Stefano Santabarbara,[1,2,3] Bradford Bullock,[4] Fabrice Rappaport,[2,*] and Kevin E. Redding[1,*]
[1]Department of Chemistry & Biochemistry, Arizona State University, Tempe, Arizona; [2]Institut de Biologie Physico-Chimique, UMR7141 CNRS-UPMC, Paris, France; [3]Istituto di Biofisica, Consiglio Nazionale delle Ricerche, Milano, Italy; and [4]Department of Chemistry, University of Alabama, Tuscaloosa, Alabama

ABSTRACT Two functional electron transfer (ET) chains, related by a pseudo-C_2 symmetry, are present in the reaction center of photosystem I (PSI). Due to slight differences in the environment around the cofactors of the two branches, there are differences in both the kinetics of ET and the proportion of ET that occurs on the two branches. The strongest evidence that this is indeed the case relied on the observation that the oxidation rates of the reduced phylloquinone (PhQ) cofactor differ by an order of magnitude. Site-directed mutagenesis of residues involved in the respective PhQ-binding sites resulted in a specific alteration of the rates of semiquinone oxidation. Here, we show that the PsaA-F689N mutation results in an ~100-fold decrease in the observed rate of PhQ_A^- oxidation. This is the largest change of PhQ_A^- oxidation kinetics observed so far for a single-point mutation, resulting in a lifetime that exceeds that of the terminal electron donor, P_{700}^+. This situation allows a second photochemical charge separation event to be initiated before PhQ_A^- has decayed, thereby mimicking in PSI a situation that occurs in type II reaction centers. The results indicate that the presence of PhQ_A^- does not impact the overall quantum yield and leads to an almost complete redistribution of the fractional utilization of the two functional ET chains, in favor of the one that does not bear the charged species. The evolutionary implications of these results are also briefly discussed.

INTRODUCTION

Photosynthetic reaction centers (RCs) are the most efficient radiation energy converters known. In particular, the quantum efficiency of photochemical charge separation in photosystem I (PSI), a large macromolecular cofactor-protein supercomplex that catalyzes the light-dependent oxidation of plastocyanin and the reduction of ferredoxin, has been estimated to be higher than 0.95 (1–3), with maximal values of ~0.97–0.99 reported in the literature (4,5). On the other hand, in the other photosystem involved in oxygenic photosynthesis, PSII, the maximal quantum efficiency has been estimated to range from 0.8 to 0.85 (6). Understanding the molecular mechanism that gives rise to such a high quantum efficiency in PSI is of pivotal interest from biological and biophysical perspectives and is important for the development of bio-inspired synthetic compounds that might be implemented in photovoltaic devices.

In contrast to the case of the better-known type II RC (6), in which a single cofactor chain is engaged in an electron transfer (ET) reaction, in PSI two parallel redox chains are active, according to what is commonly referred to as a bidirectional ET mechanism (7,8). The PSI structural models (9,10) clearly identify the ET cofactors, which are organized into two symmetric chains with respect to the pseudo-C_2 symmetry axis parallel to the membrane plane. This is a common structural feature of all photosynthetic RCs whose structure is known (i.e., the purple bacterial RC (11,12), PSI (9,10), and PSII (13,14)). The photochemical and redox active cofactors are principally coordinated by the RC subunits PsaA and PsaB, which form a transmembrane heterodimer. The terminal iron-sulfur clusters, F_A and F_B, are bound to the extrinsic PsaC subunit. Each ET chain (ETC) is primarily, although not exclusively, coordinated by one of the two main RC subunits, and therefore the two chains are referred to here as ETC_A and ETC_B. Charge separation and successive radical pair stabilization reactions take place in a cluster of six chlorophyll (Chl) *a* molecules (1–3,7). Two of these Chls form a Chl dimer coordinated at the interface of the PsaA/PsaB heterodimer, which is known as P_{700}. The other four Chls are organized symmetrically into two pairs, referred to here as $ec2_A/ec3_A$ and $ec2_B/ec3_B$. Charge separation has been considered to initiate at the level of the P_{700} excited state, thereby acting as the primary electron donor (1,7,15,16). More recently, it was shown that charge separation takes place independently within each ec2/ec3 pair (17,18). The ec3 Chls are generally considered to be the primary electron acceptors (also known as A_0) (1,7,15–18). Irrespective of the detailed mechanism of charge separation, the radical pair $[P_{700}^+A_0^-]$ is populated in a few tens of picoseconds (1,3,7,15–18), followed in <100 ps by a reduction of the phylloquinone (PhQ) on the utilized branch (PhQ_A or PhQ_B), also known as A_1 (7,8,19). The quinone in turn

Submitted October 29, 2014, and accepted for publication January 7, 2015.
*Correspondence: kevin.redding@asu.edu or fabrice.rappaport@ibpc.fr
Editor: Simon Scheuring

0006-3495/15/03/1537/11 $2.00
http://dx.doi.org/10.1016/j.bpj.2015.01.009

reduces F_X, an interpolypeptide [4Fe-4S] cluster where ETC_A and ETC_B converge.

Whereas the two ETCs present in PSI are functional and are used at a similar level, with possible variations among species (19–27), they are not functionally identical. Different kinetics have been suggested at the level of primary charge separation/stabilization events (18) and, even more obviously, in oxidation of the phyllosemiquinone (PhQ^-): the lifetimes attributed to $PhQ_A^- \rightarrow F_X$ and $PhQ_B^- \rightarrow F_X$ differ by an order of magnitude i.e., ~250 ns and ~20 ns, respectively (7,8,19–21). As the cofactors bound to each ETC are chemically identical, and the inter-cofactor distances differ only by fractions of an Ångstrom, the distinct kinetics of ET must stem from subtle differences in the interactions of the cofactors with their binding niches that finely tune the physicochemical properties of the redox moieties. This is illustrated by the fact that a single amino acid substitution can cause PhQ^- oxidation kinetics to vary over a wide range, either increasing (19–23,27–30) or decreasing (31–33) the oxidation lifetime. A clear example of protein-mediated tuning of redox cofactor properties was provided by mutation analyses of the PhQ_A binding niche, the oxidation lifetime of which was shown to vary from ~150 ns to 1.5 μs in response to single residue substitution (7,8,19–23,31–33).

It has also been shown that substitution of single residues involved in the coordination of the $ec3_A$ or $ec3_B$ cofactors, which are located upstream of the PhQ in ETC_A or ETC_B, respectively, affects the fraction of electrons transiting through each branch (18,24–28,34,35). Moreover, functional studies of double mutants that combine mutations affecting the coordination of $ec3_A$ and PhQ_A demonstrated that their effects are additive (30). Hence, the functional symmetry of the system appears to be rather plastic, since a few selected amino acid substitutions can change the properties of the two individual ETCs significantly without affecting the functionality of the ensemble. This is particularly interesting when placed in an evolutionary perspective, since type I and type II RCs are thought to share an ancestor that was homodimeric and hence symmetrical (36).

Here, we present the analysis of a mutation in the PhQ_A binding pocket (PsaA-F689N) in PSI of *Chlamydomonas reinhardtii* (see Fig. 1 *A*), which slows down PhQ_A^- oxidation kinetics by almost two orders of magnitude. This creates an unprecedented situation in which the reduction of P_{700}^+ is faster than the oxidation of the semiquinone, thereby providing the opportunity to initiate a second photochemical event while PhQ_A^- is still present in ETC_A. We show that the probability for ET to occur down ETC_A is dramatically decreased while PhQ_A is reduced, and that this decrease is compensated for by the increased occurrence of ET down ETC_B so that the overall yield of charge separation remains unaffected. This further illustrates the functional plasticity that we propose is inherent to the (co)existence of the two ETCs and may have allowed evolutionary tinkering while preserving the function of the RC.

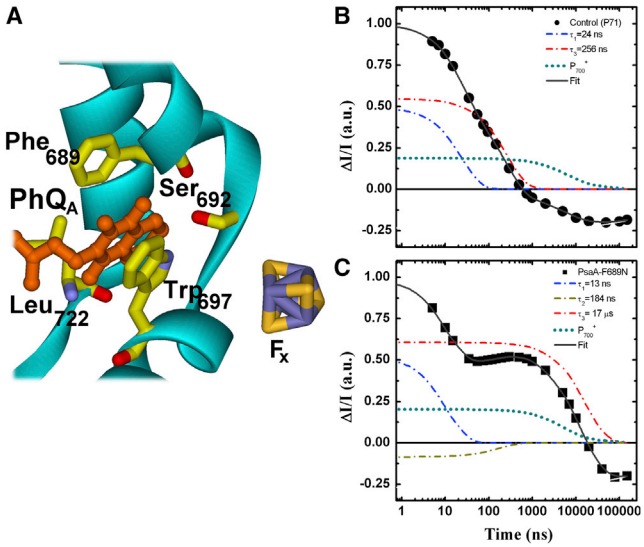

FIGURE 1 (*A*) Schematic representation of the binding site for PhQ_A (*orange*), highlighting the main cofactor-protein interactions. Also shown is the iron-sulfur center F_X (S: *yellow*, Fe: *violet*). (*B* and *C*) Kinetics of PhQ^- oxidation monitored at 395 nm in the control strain (*B*) or PsaA-F689N mutant (*C*). Solid symbols are the experimental results and the thick solid line is the fit to a sum of exponential functions. Also shown are the contributions of the decay components ascribed primarily to oxidation of PhQ_B^- (*blue*, 24 ns in the WT and 13 ns in the mutant), oxidation of PhQ_A^- (*red*, 256 ns in the WT and 17 μs in the mutant), inter-FeS cluster ET (*gold*, 184 ns in the mutant), and reduction of P_{700}^+ (the latter is actually the sum of the ~6 μs and ~55 μs components). Note that the ~180 ns component due to inter-FeS cluster ET is not resolvable in the WT. Data are normalized on same total amplitude and same initial intensity. To see this figure in color, go online.

MATERIALS AND METHODS

Creation of the PsaA-Phe689 substitution mutants

Mutant strains were constructed as previously described (37). Briefly, site-directed mutations were constructed by PCR using plasmids designed to re-insert the *psaA-3* gene (38). Plasmids bearing mutations in codon 689 of *psaA* exon 3 (*psaA-3*) were introduced into strain KRC91-1A (*P71 psbAΔ psaA-3Δ*) via the bio-ballistic method, followed by selection for resistance to spectinomycin and streptomycin. This strain has low expression of antenna proteins due to the *P71* nuclear mutation, and lacks PSII due to the deletion of the *psbA* gene, which encodes the D1 core polypeptide. All transformants were grown under low continuous illumination (~10 $\mu E\ m^{-2}\ s^{-1}$) in Tris-acetate-phosphate medium (39).

Transient optical spectroscopy

Pump-probe experiment

We monitored the kinetics of ET after a single-turnover laser-flash excitation by time-resolved difference absorption spectroscopy using an in-house-built pump-probe setup previously described in detail (40). In brief, the pump flash (centered at 700 nm) is provided by a dye (LDS 698) laser pumped by the second harmonic of an Nd:YAG laser (Brilliant; Quantel).

The tunable probe pulses are obtained from an optical parametric oscillator (Panther; Continuum) pumped by the third harmonic of an Nd:YAG laser (Surelite II; Continuum). In both cases, the pulse duration is ~5 ns, the intensity of the pump is attenuated so as to excite ~70% of the RCs, and the probe is attenuated to avoid actinic effects. The pump intensity is sufficiently low to avoid multiple turnovers and nonlinear absorption processes. The pump-probe delays are controlled by a programmable in-house-built pulse sequencer.

Pump-pump-probe experiment

The setup described above was modified to perform pump-pump-probe experiments. The first actinic flash was provided by an optical parametric oscillator (SLOPO; Continuum) pumped by the third harmonic of an Nd:YAG laser (Surelite II; Continuum). The second pump flash and the probe flash were as described above. The delay between the first and second pump pulses was controlled by an electronic delay unit (Stanford) triggered by the same pulse programmer described above.

Data analysis

The kinetics recorded at multiple detection wavelengths were fitted globally by a sum of exponentials as previously described (31,41). The plot of the amplitude as a function of wavelengths yields the decay-associated spectra (DAS). Goodness of fit is judged by the reduced χ^2, inspection of residual plots, and cross-correlation analysis. The data presented are the averages of at least four independent data sets.

Kinetic modeling

The kinetics of secondary ET reactions were modeled as previously described (7,29,31) by solving a system of linear differential equations. Further details are provided in the Supporting Material.

RESULTS

Kinetic characterization of the PsaA-F689N mutation

The kinetics of PhQ^- oxidation (monitored at 395 nm) in the PsaA-F689N mutant of *C. reinhardtii* are shown in Fig. 1 *C* and compared with a control strain harboring wild-type (WT) PSI (Fig. 1 *B*). Also shown are the fits to the experimental data by a sum of exponential functions and the contribution of each exponential phase to the total decay. These different components were obtained by a global fit of the individual kinetics recorded at several wavelengths, from which the DAS were retrieved (shown in Fig. 2). As some components are markedly slower in the PsaA-F689N mutant compared with the WT, we extended the time range to hundreds of microseconds for both strains. The investigated time window therefore exceeded four orders of magnitude, requiring four kinetic components in the WT and five components in the mutant to obtain good fits.

In the WT, two exponential components fall in the submicrosecond time range, with lifetimes of 24 ± 2 ns and 256 ± 6 ns, as previously observed in PSI of *C. reinhardtii* (7,8,17). These are primarily due to the oxidation of PhQ_B^- and PhQ_A^-, respectively. Two exponential decay components were required in the microsecond time window (6.2 ± 0.9 μs and 56 ± 3 μs). Based on their lifetimes and DAS (Fig. 2, *B* and *D*), these are assigned to the reduction of P_{700}^+ by prebound or unbound plastocyanin, respectively (41).

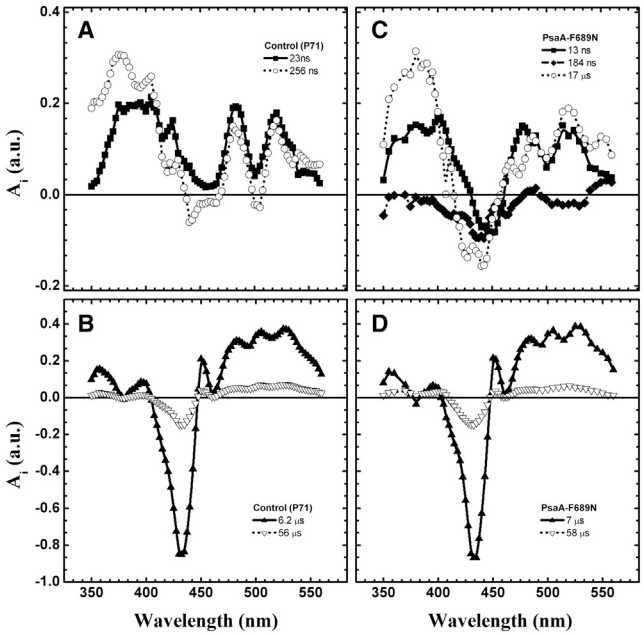

FIGURE 2 (*A–D*) DAS retrieved from global analysis in the nanosecond-to-microsecond timescale using control (*A* and *B*) or PsaA-F689N (*C* and *D*) cells. (*A*) 24 ns (*solid squares*) and 256 ns (*open circles*) components in the WT. (*B*) 6 μs (*solid triangles*) and 56 μs (*open triangles*) components in the WT. (*C*) 13 ns (*solid squares*), 184 ns (*solid diamonds*), and 17 μs (*open circles*) components in PsaA-F689N. (*D*) 7 μs (*solid triangles*) and 58 μs (*open triangles*) components in PsaA-F689N.

In the PsaA-F689N strain of *C. reinhardtii*, the kinetics are described by a sum of five exponential decay components with lifetimes of 13 ± 3 ns, 184 ± 4 ns, 7 ± 1 μs, 17 ± 2 μs, and 58 ± 5 μs. The components with lifetimes of 7 and 58 μs are similar in terms of both lifetime and DAS to the corresponding ones obtained with the control strain (Fig. 2 *D*), and thus are assigned to P_{700}^+ reduction as well. The three remaining components (13 ns, 184 ns, and 17 μs) are specific to the mutant. The DAS associated with the 13 ns and 17 μs components in PsaA-F689N exhibit significant positive absorption in the near-UV region and their band shapes are similar to the DAS of the 24 ns and 256 ns components, respectively, observed in the WT PSI and assigned to PhQ^- oxidation (Fig. 2, *A* and *C*).

The lifetime of the fastest component, which is ascribed mainly to the oxidation of PhQ_B^- by F_X, is in the range commonly reported for this reaction (7,8,18–23,28–32), albeit somewhat on the low end of the spread. The DAS of the 17 μs component displays significant amplitude in the near-UV region and a feature corresponding to an electrochromic signal in the 450–550 nm spectral window. Thus, this component is assigned to the oxidation of PhQ_A^-, making it almost two orders of magnitude slower than in the WT

(200–300 ns). Several studies have shown that single mutations in the PhQ_A binding pocket can slow down the kinetics of PhQ_A^- oxidation (22,23,28,29), but the change rarely exceeded 5-fold (7,8,18–23). Although a remarkable slowing of PhQ_A^- oxidation was also observed in mutants of the PhQ biosynthetic pathway, leading to the replacement of PhQ by plastoquinone (or other exogenous quinones) in the PhQ site of PSI (19), the effect seen in the PsaA-F689N mutant is by far the largest described to date for a single-residue substitution of a RC subunit residue harboring the endogenous PhQ.

In the PsaA-A689N mutant, an additional kinetic component is detected with a lifetime of 184 ± 4 ns. Kinetic components with similar lifetimes, falling in the 150–200 ns range and exhibiting similar DAS, were previously observed in other mutants that slow PhQ_A^- oxidation and were assigned to ET from F_X to F_A/F_B (28,30). The presence of a kinetic phase with a lifetime intermediate between those ascribed principally to PhQ_A^- and PhQ_B^- oxidation was also observed in a temperature-dependence study in the WT PSI (21,41,42). However, this component is not resolved in measurements performed at a single temperature, due to its low relative amplitude and temporal overlap with the ~250 ns component. Thus, as previously discussed (28,30), the ~250 ns component in WT PSI will contain spectral changes due to both PhQ_A^- oxidation and intra-FeS cluster ET.

Kinetics of ET studied by pump-pump-probe experiments

A remarkable consequence of the PsaA-F689N mutation is that it makes the oxidation of PhQ_A^- slower than the P_{700}^+ reduction, 85% of which is reduced with a ~6 μs lifetime by prebound plastocyanin (Fig. 2) (41). This opens up the possibility of exploring the photochemical activity of PSI under conditions where PhQ_A is present in the semiquinone state. This would mimic what occurs in type II RCs, where the second charge separation occurs in the presence of a semiquinone anion (at the Q_B site), as two successive photochemical acts are required for its double reduction and protonation (6). To study secondary ET after initiation of photochemistry in the PSI RC containing PhQ_A^-, we designed a novel (to our knowledge) experimental setup that is based on double laser-flash excitation and hence consists of a pump-pump-probe sequence, as opposed to the classical pump-probe experiment. The first actinic excitation prepares the system in a given redox state and the second actinic excitation induces a second charge separation in the context of that state. One can then assess the consequence(s) of the presence of PhQ_A^- by comparing the kinetics of the individual reactions measured after one or two actinic flashes.

Fig. 3 shows the kinetics of PhQ^- oxidation, monitored at 395 nm in the control (A) and PsaA-F689N mutant (B) strains,

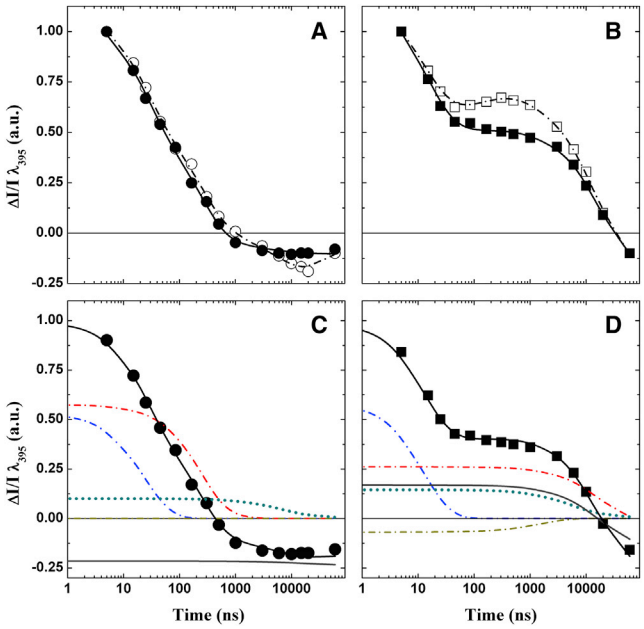

FIGURE 3 (*A* and *B*) Comparison of kinetics monitored at 395 nm in pump-pump probe and pump-probe experiments in the WT (*A*) and PsaA-F689N (*B*) strains, using a pump-pump delay (Δ*T*) of 15 μs. The solid symbols and solid lines are the data and fits, respectively, for the pump-pump probe experiment. The open symbols and dashed lines show the experimental kinetics and fits, respectively, for the classic pump-probe experiment. (*C* and *D*) Fit of the pump-pump-probe data at 395 nm for the WT (*C*) and PsaA-F689N (*D*) strains. The solid lines are the fits to the data sets; the contributions of different decay phases are also shown. (*C*) 24 ns (*dash-dotted blue line*), 258 ns (*dash-dotted red line*), sum of the 6 μs and 56 μs (*dotted green line*) phases attributed to P_{700}^+ reduction, and sum of the decay tail elicited from the first pump pulse in the sequence (*thick gray line*). (*D*) 13 ns (*dash-dotted blue line*), 17 μs (*dash-dotted red line*), 184 ns (*dash-dotted golden line*), sum of 7 μs and 58 μs phases of P_{700}^+ reduction (*dotted green line*), and sum of the decay tail from the first pump pulse in the sequence (*thick gray line*). The traces are normalized to the same total amplitude (extrapolated to t_0) and the same offset to facilitate comparison. To see this figure in color, go online.

obtained after either the pump-probe or the pump-pump-probe sequence with a delay of 15 μs between the two pump flashes. The data were fitted by the function $f(t) = x \cdot (\sum_{j=1}^{n} A_j \cdot e^{-t/\tau_j}) + (1-x) \cdot (\sum_{i=1}^{n} A_i \cdot e^{-(t+\Delta T)/\tau_i}) + A_\infty$, where τ_i and τ_j are the lifetimes; A_i and A_j are the relative amplitudes of each individual component in the pump-probe (i) and pump-pump-probe (j) experiments, respectively; and x is the molar fraction of centers that effectively perform a second charge separation upon the second pump flash. It is worth noting that x is equivalent to the fraction of centers in which P_{700} is reduced at the moment of the second pump flash, and that it can be retrieved from the pump-probe data set described above. The same is true for the values of A_i and τ_i, which significantly decreases the number of fit parameters.

In the case of the control strain, the amplitude-normalized transient absorption kinetics monitored at 395 nm with a pump-pump delay of 15 μs hardly differed from that obtained after a single actinic flash (Fig. 3 *A*). In contrast,

the kinetics obtained by the two protocols differed markedly in the PsaA-F689N mutant (Fig. 3 *B*) and became significantly faster overall in the pump-pump-probe experiment compared with the pump-probe kinetics. Fitting of the data with the expression described above (Fig. 3 *D*) indicates that whereas the lifetimes remained unaltered (within the parameter confidence bounds), the amplitude of the 13 ns phase increased significantly with respect to the 17 μs phase, shifting the ratio of fast/slow phases of PhQ^- oxidation from 0.41:0.59 to 0.62:0.38. This represents a 50% increase of the relative amplitude of the 13 ns component, with a concomitant 35% decrease of the 17 μs phase, corresponding to a significant overall redistribution in the kinetic components. It is important to consider that for a pump-pump delay of 15 μs, a significant fraction of PSI RCs will have relaxed to a state in which all ET cofactors are in the ground state. Based on the kinetics of P_{700}^+ reduction and PhQ^- oxidation, this relaxed fraction would account for ~80% of the RCs that are capable of performing stable charge separation (i.e., in which P_{700} is in its neutral state). The increase of the 13 ns phase from 41% to 62% in the pump-pump-probe kinetics is thus remarkably close to the predicted fraction of photochemically active RCs containing PhQ_A^-, indicating that the majority of ET leads to the reduction of PhQ_B (for a more in-depth description, see Fig. S3).

The relative increase of the 13 ns phase with respect to the 17 μs phase was observed at several monitoring wavelengths in the PsaA-F689N mutant in the double-pump experiment. This is shown in Fig. 4, where the relative amplitudes of the fast PhQ^- oxidation phase in the pump-probe and pump-pump-probe experiments at selected wavelengths (395, 430, 445, and 480 nm) are compared. The relative increase of the 13 ns phase in PsaA-F689N was similar at all wavelengths tested (Fig. 4 *B*). This was not the case for WT PSI (Fig. 4 *A*), where smaller changes of variable sign were observed.

This consistency of the relative increase of the 13 ns phase is especially significant at 445 nm, as this wavelength is a sensitive indicator of charge recombination of the $P_{700}{}^+A_0{}^-$ radical pair (28,43,44). The charge recombination process occurs with a lifetime of ~20–40 ns and overlaps temporally with the fast PhQ^- oxidation phase (7,8,15,28,43). However, the DAS associated with the $P_{700}{}^+A_0{}^-$ charge recombination process is markedly different from that of PhQ^- oxidation. Therefore, if charge recombination were to occur, it would lead to an alteration of the DAS (and lifetime) of the fastest PhQ^- oxidation component, especially at 445 nm, as previously observed in mutants that promote $P_{700}{}^+A_0{}^-$ recombination (28,30,44). However, such changes were not observed here (see Fig. S2). On the contrary, the increase of the relative amplitude of the 13 ns component is more pronounced at 395 nm (PhQ^- absorption) and 480 nm (electrochromic band shift; Fig. 4 *B*), both of which are marker

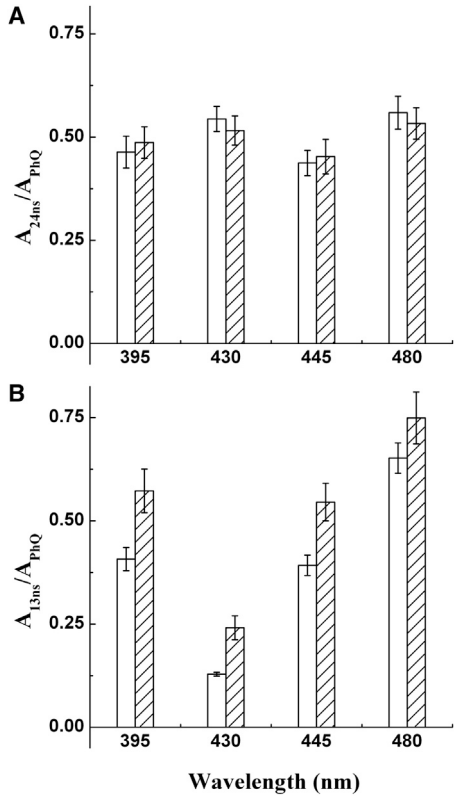

FIGURE 4 The fractional amplitude of the faster PhQ^- oxidation component (24 ns for the WT and 13 ns for PsaA-F689N) to the total amplitude of PhQ^- oxidation is shown as a function of wavelength for both the pump-probe (*open*) and pump-pump-probe (*hatched*) experiments. (*A*) WT. (*B*) PsaA-F689N mutant. Error bars are the propagation of the standard deviation of the mean values.

wavelengths for processes associated with forward ET rather than charge recombination.

Therefore, the best explanation for the increase in the relative amplitude of the 13 ns component in pump-pump-probe experiments is an increase in the relative yield of the photochemical reduction of PhQ_B^- when PhQ_A^- is present in the ETC_A chain. We further tested this hypothesis by measuring the relative amplitude of the PhQ^- oxidation phases as a function of the delay between the two pump flashes. In this framework, it is expected that 1) the total number of open centers that can perform charge separation will increase as plastocyanin reduces P_{700}^+ produced by the first flash (i.e., with time constants of ~6 μs and ~55 μs), and 2) the ratio of the fast and slow phases of PhQ^- oxidation after the second flash will decrease as PhQ_A^- is oxidized by F_X (i.e., with a time constant of ~17 μs). The experimental kinetics at 390 nm at pump-pump delays (ΔT) are shown in Fig. 5 *A*, while Fig. 5 *B* shows the dependence of the relative amplitude of the fast phase (A_{fast}) and the total signal (A_{tot}) as a function of ΔT. As expected, A_{tot} increased as a function of the pump-pump delay, and its time dependency can be described by the function $A_{tot} = (1 - e^{-\tau_B/t})$, with τ_B ~11 μs. This value is close to

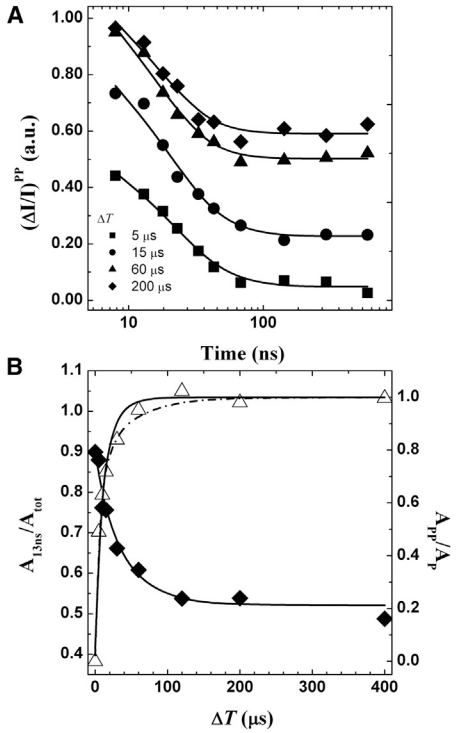

FIGURE 5 (*A*) Initial decay of the absorption difference signal at 390 nm in pump-pump-probe experiments in the PsaA-F689N mutant, using different values of ΔT: 5 μs (*squares*), 15 μs (*circles*), 60 μs (*triangles*), and 200 μs (*diamonds*). The symbols and lines are the data and fits, respectively. (*B*) Dependence of the total signal amplitude (*open triangles*, left *y* axis) and the ratio between the fast phase of PhQ^- oxidation and the total signal amplitude (*solid diamonds*, right *y* axis) as a function of ΔT. The increase of total signal amplitude is described by either a monoexponential recovery with $\tau_B = 11 \pm 1$ μs (*solid line*) or a biexponential recovery with $\tau_{B,1} = 6 \pm 1$ μs and $\tau_{B,2} = 62 \pm 4$ μs (*dash-dot line*). The A_{fast}/A_{tot} (ΔT) ratio is described by an exponential decay with a lifetime of 20 ± 3 μs.

the average lifetime of P_{700}^+ reduction, when the contributions of the ~6 μs and ~55 μs components are weighted by their fractional amplitudes. In fact, a closer match to the experimental data is obtained by a biexponential fit (Fig. 5 *B*), yielding lifetimes of $\tau_{B,1} = 6 \pm 1$ μs (72%) and $\tau_{B,2} = 62 \pm 4$ μs (28%), which is fully consistent with A_{tot} representing the fraction of PSI with neutral P_{700} (i.e., open) when the second pump pulse excites the RC.

The fractional amplitude of the ~13 ns phase of PhQ^- oxidation (A_{fast}/A_{tot}) decreases monotonically as a function of pump-pump delay ΔT, approaching a final value similar to that seen in the simple pump-probe experiment. Its time dependency can be described by a single exponential decay with a lifetime of ~20 μs (Fig. 5 *B*), which is close to the 17 μs lifetime of PhQ_A^- oxidation measured in the PsaA-F689N mutant by the pump-probe experiment. Since it is possible to exclude the notion that the increase in the relative amplitude of the 13 ns phase is due to charge recombination of $P_{700}{}^+A_{0A}{}^-$, it must therefore reflect the redistribution of the statistical utilization of ETC_A and ETC_B, from a ratio of ~0.4:0.6, under neutral conditions, to larger than 0.9:0.1 under conditions of charge separation occurring in the presence of PhQ_A^-.

Simulation of the pump-pump kinetics in PsaA-F689N

To gain further insights into the redistribution of utilization of ETC_A and ETC_B caused by the presence of PhQ_A^-, we performed a simulation of the kinetics based on a few simple rationales. The simulations consider that when the second pump pulse excites the sample at any delay time (ΔT) longer than ~100 ns after the first actinic flash (i.e., after complete oxidation of PhQ_B^-), PSI can be present in four possible redox states: 1) the fraction in which the primary donor (P_{700}) is oxidized and the secondary acceptor (PhQ_A) is reduced is denoted as $\sigma_{P_{700}^+PhQ^-}$, 2) the fraction in which both P_{700} and PhQ_A are oxidized is denoted as $\sigma_{P_{700}^+PhQ}$, 3) the fraction in which P_{700} is reduced and PhQ_A is oxidized is denoted $\sigma_{P_{700}PhQ}$, and 4) the fraction in which both P_{700} and PhQ_A are reduced is denoted $\sigma_{P_{700}PhQ^-}$. The probability that a particular PSI RC will be in any of these states depends on the kinetics with which each of the cofactors returns to its neutral state after photochemical oxidation/reduction. The molar fractions of the various redox states described above are then equivalent to the combinatorial probability of the population evolution of the individual cofactors (presented in Fig. S3).

The pump-pump-probe kinetics are modeled according to the following assumptions (for a more in-depth discussion, see Supporting Material).

1. When the electron donor is oxidized (i.e., P_{700}^+), the system cannot undergo charge separation (i.e., it is closed). Therefore, fractions $\sigma_{P_{700}^+PhQ^-}$ and $\sigma_{P_{700}^+PhQ}$ will not contribute to the light-induced signal.
2. In the $\sigma_{P_{700}PhQ}$ fraction of centers, the system is in its relaxed state and the evolution of the state produced by the second pump flash is identical to that observed with a single flash in the submicrosecond timescale, with the exception of the P_{700}^+ reduction kinetics. The ratio of the fast (6 μs) and slow (55 μs) phases of P_{700}^+ reduction slightly differs from that observed after the first flash, because the dissociation of oxidized plastocyanin and association of reduced plastocyanin occur within the microsecond timescale (see Supporting Material for more details).
3. In the $\sigma_{P_{700}PhQ^-}$ fraction, the presence of PhQ_A^- will modify the energetics of charge separation in ETC_A (e.g., by Coulombic interactions), causing a complete redistribution in favor of ETC_B. It is assumed (for the sake of simplicity) that the ET rates through the B-branch and to the FeS clusters will not be significantly different due to the presence of PhQ_A^-.

Part of the absorption difference signal detected at long delays in whole cells is due to late electron transport

events and is described in the analysis by a nondecaying component (e.g., Fig. 1, *B* and *C*). Since the intensity of the nondecaying signal in a pump-pump-probe experiment is not predictable in a straightforward manner, it was allowed to vary in the simulation to enable a closer match to the experimental data, as it does not affect the kinetics in the investigated time window (further details are given in Fig. S4 and the Supporting Material). The results of the simulation of the kinetics in the PsaA-F689N mutant made under these assumptions are shown in Fig. 6, where it can be seen that they satisfyingly agree with the experimental results.

Based on the same rationale, it is possible to simulate the ΔT dependence of the pump-pump-probe signal (Fig. S5). There are two implications to the striking agreement between the simulations and the experimental results. First, it confirms that $P_{700}{}^{+}A_0{}^{-}$ charge recombination is not taking place to a significant extent during the pump-pump-probe experiments in the PsaA-F689N mutant. Such a good agreement between simulated and experimental kinetics would be possible only in the case that $\Delta\varepsilon_{[P_{700}^{+}A_0^{-}]-[P_{700}A_0]} = \Delta\varepsilon_{Ph^{-}-Ph}$ at 395 nm, and a comparison of the DAS attributed to P_{700}^{+} and PhQ^{-} (i.e., Fig. 2) indicates that this is not the case. Second, it strongly suggests that the presence of PhQ_A^{-} at the moment that charge separation takes place leads to an almost complete redistribution of primary charge separation probabilities between the two active ETCs of PSI, favoring initial photochemistry in ETC_B.

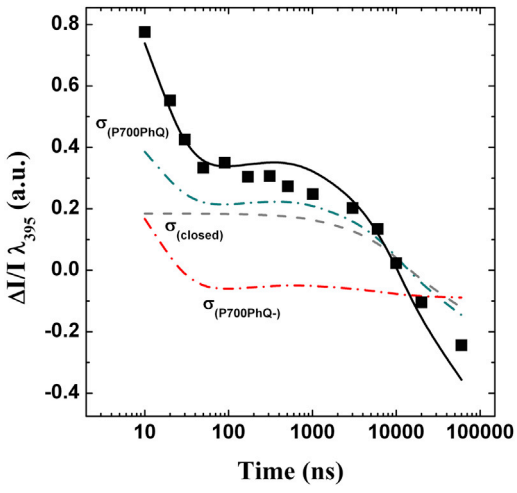

FIGURE 6 Simulation of pump-pump-probe kinetics in the PsaA-F689N mutant. The simulations (*black line*) are based on the fit of the pump-probe data (Fig. 1) and are compared with the experimental results (*squares*; as in Fig. 3, but without amplitude normalization). Also shown is the deconvolution of the contributions to the pump-pump-probe absorption difference kinetics from the various redox state fractions of the RC at the time of the second pump pulse: $\sigma_{P_{700}PhQ^{-}}$ (*dash-dotted red line*), $\sigma_{P_{700}PhQ}$ (*dash-dotted blue-green line*), and σ_{closed} (*dashed gray line*). To see this figure in color, go online.

DISCUSSION

Effect of the PsaA-F689N mutation on forward ET kinetics

The PsaA-F689N substitution causes a significant increase of the lifetime of PhQ_A^{-} oxidation, from ~250 ns in the WT to 17 μs in the mutant (Fig. 1). This effect is more than one order of magnitude greater than those previously observed as a result of a point mutation affecting the protein environment of the PhQ_A-binding site (7,8,18–23). Although there remains some disagreement concerning the effective midpoint of PhQs in PSI (7,15,19,21,45–49), it has been shown that both the WT kinetics and the effect of mutations in the PhQ_A binding site can be rationalized on a semiquantitative basis by a model that considers the oxidation of PhQ_A^{-} to be energetically uphill and that of PhQ_B^{-} to be downhill (7,21,27,29,31). The lifetime observed in the PsaA-F689N mutant can be qualitatively explained, with all other energetic parameters being unchanged from those of the WT, by a ~100-fold increase of the equilibrium constant, corresponding to an upshift by ~125 mV of the midpoint potential of the PhQ_A^{-}/PhQ_A couple (Fig. S1; Table S1). This description reproduces the experimental lifetimes of both the slower component (17 μs) and the smaller time constant for the faster decay component. However, the amplitude associated with the slow phase is significantly overestimated in the simulations for the PsaA-F689N mutant (ratio of ~0.96:0.04; Table S1) compared with the relatively modest fractional increase of this component observed experimentally, which is 0.75:0.25 on average, using the kinetics monitored in the 360–400 nm range (Fig. 2).

Even though the kinetics simulations should be considered only a semiquantitative description of the system, previous descriptions of PhQ_A-binding-site mutants that considered the variation of the PhQ_A/PhQ_A^{-} redox potential as the sole mutation-induced perturbation to the energetic parameters that control ET yielded a rather satisfactory description of both the experimental lifetimes and associated amplitudes (7,21,27,29,31). Thus, the discrepancy between simulations and experimental results for the PsaA-F689N substitution suggests that the mutation does not solely affect the PhQ_A^{-} redox potential. Among the other parameters that would affect the ET rates, one may consider an increase in the (total) reorganization energy (λ_{tot}) from a value of 0.7 to 1 eV for $PhQ_A^{-} \rightarrow F_X$. These values fall in the range commonly reported for ET proteins, including PSI (7,15,42,50–52). This, combined with an upshift of the PhQ_A^{-}/PhQ_A midpoint potential of 105 mV, results in a good prediction of the lifetimes, as well as the fractional amplitude of the slow/fast phase of PhQ^{-} oxidation (~0.81:0.19; Table S1).

Although the parameters retrieved from kinetic modeling should be considered only as semiquantitative, because of

the unavoidable approximations required in the calculations, the simulations nonetheless indicate that a shift of the PhQ_A^- potential by at least ~100 mV is induced by the PsaA-F689N mutation. Therefore, irrespective of the midpoint potential of PhQ_A^- considered for the WT, which has been reported as being in the range of ± 120 mV that of F_X (7,15,19,21,45–49), the mutation-induced perturbation would render the $PhQ_A^- \rightarrow F_X$ reaction in PsaA-F689N as energetically either barely downhill or significantly uphill.

Modulation of ET directionality within PSI by the presence of PhQ_A^-

The amplitude of the fast PhQ^- oxidation phase, which, as established by previous studies (18,53), can be taken as a reliable measure of ETC_B utilization, is strongly increased if PhQ_A^- is present when charge separation is initiated. We have already discussed the assignment of this component to the oxidation of PhQ_B^- rather than to charge recombination of $P_{700}{}^+A_0{}^-$. Notably, our normalization procedure uses the total amplitudes obtained after the first pump flash as an internal standard. Although this does not represent an absolute estimate of the photochemical quantum efficiency, which for PSI of higher plants approaches unity (4,5), it allows us to rule out any significant change in quantum efficiency in pump-pump-probe experiments performed in the PsaA-F689N mutant. Consistent with this, the data can be simulated assuming that the redistribution in favor of ETC_B is close to 100% (Fig. 6; Supporting Material).

Charge recombination from the so-called stabilized radical pair $P_{700}{}^+A_0{}^-$ occurs in ~20–40 ns and leads to the repopulation of the RC excited state, as well as the ground and triplet states ($^3P_{700}$). Whereas the excited state can be retrapped with high probability by the ETC_B cofactors, thereby promoting a redistribution of the chain utilization without a significant reduction of the quantum yield, repopulation of the ground state or the population of $^3P_{700}$ would instead be photochemically unproductive, thereby lowering the quantum efficiency by some significant extent. Since, as discussed above, we did not observe such a decrease, redistribution is unlikely to involve repopulation of the excited state from a relatively long-lived radical pair (e.g., $P_{700}{}^+ec3_A{}^-$) that would have been formed on the A branch.

The most straightforward hypothesis to explain our results is that the charge borne by PhQ_A^- modifies the standard free-energy difference (ΔG^0) between the initial radical pair produced by charge separation and the RC excited state, disfavoring its formation (and/or favoring the backward repopulation of the RC excited state). Such an electrostatic effect would not be unprecedented, since similar conclusions were reached regarding the energetics of charge separation in PSII in the presence of Q_A^- (54). In addition, this interpretation is consistent with the proposal advanced by Müller et al. (18) that the statistical utilization of the two ETCs is determined by the competition for conversion of the excited state into either $ec2_A{}^+ec3_A{}^-$ or $ec2_B{}^+ec3_B{}^-$, which are considered to be the primary radical pair states in their model. The effects of mutations that alter the redox properties of $ec3_A$ or $ec3_B$ by breaking a hydrogen bond (H-bond) to the 13^1 keto oxygen of the targeted Chl, leading to a partial redistribution of the statistical utilization of ETC_A/ETC_B (18,53), were described in terms of a decrease of ΔG^0 of initial charge separation from –90 meV in the WT to approximately –70 meV in the mutants (18). The apparent effect on directionality observed in the PsaA-F689N mutant when photochemistry was performed in the presence of PhQ_A^- seems to be significantly larger than that observed in these point mutants of the ec3 Chl-binding sites in PSI of *C. reinhardtii* (18,28,53). Thus, the change in ΔG^0 associated with primary radical pair formation in the presence of PhQ_A^- would need to be larger than the change caused by the H-bond mutants. This is reasonable in light of the facts that the center-to-center distance between PhQ_A and $ec3_A$ is ~9 Å, and the dielectric constant associated with membrane proteins is typically considered to be low (in the 4–20 range), leading to fairly large electrostatic interactions (i.e., ~80–400 meV). These are larger perturbations than would be expected from the disruption of a single H-bond to the 13^1-keto group of a Chl *a* (18,30,53,55). Hence, although the mechanisms of primary charge separation and the associated energetics in PSI are still under debate (1,7,17,18,49,56), Coulombic interactions in the range of 80–400 meV would likely affect the charge separation kinetics on ETC_A even when one considers larger values of ΔG^0 for charge separation (under normal conditions) than those estimated by Müller et al. (18). Therefore, regardless of the exact mechanism considered, electrostatic repulsion would decrease the driving force for charge reparation on ETC_A significantly, thereby favoring trapping by ETC_B, in agreement with the experimental observations reported here. This represents a novel (to our knowledge) mechanism of directionality control in photosynthetic RCs.

Insights into the evolution of photosynthetic RCs

These results provide insights into the evolution of photosynthetic RCs, from a bioenergetics perspective. In type II RCs, initial charge separation is fully asymmetric (unidirectional) and the lifetime of the Q_B semiquinone form is such that it is compatible with the double reduction (and protonation) of the terminal quinone through the $Q_A^-Q_B^- \rightarrow Q_AQ_B^{2-}$ reaction, which occurs after a second charge separation event. If indeed, as is commonly agreed upon, type I and type II RCs evolved from a common ancestor that was homodimeric, there should be a reasonable scenario describing their progressive evolution. Gene duplication represents a decisive initial step, as it made possible the divergent evolution of the two subunits that

make the heterodimer constituting the core of all known type II RCs.

In concert with previous work, the results presented here provide some rationales on which the evolutionary scenario may have relied to convert a type I-like RC into a type II-like RC, involving relatively few single amino acid substitutions. First, as previously demonstrated (7,8,18–23), a single amino acid substitution can lead to a significant increase in the semiquinone lifetime; here, we show that an increase of 2 orders of magnitude can be achieved from a single amino acid substitution (~17 μs in PsaA-F689N compared with ~250 ns in the WT). A lifetime in the hundreds of microseconds time range, as in the case of in type II RCs (6), would not require much additional change. We interpret the increased lifetime of PhQ_A^- resulting from the PsaA-F689N substitution as (predominantly) upshifting the reduction potential of the PhQ_A/PhQ_A^- couple. This also implies a large difference in the E^0 value between PhQ_A/PhQ_A^- and PhQ_B/PhQ_B^- couples, and thus a large driving force for interquinone ET mediated by F_X, according to the reaction scheme $PhQ_B^-F_XPhQ_A \rightarrow PhQ_BF_X^-PhQ_A \rightarrow PhQ_BF_XPhQ_A^-$, which has been proposed to occur in WT PSI (21,31). The oxidation of PhQ_A^- is thus thermodynamically driven by coupling with the large exergonic oxidation of F_X^- by F_A/F_B(7,15,19). Therefore, in the absence of F_A/F_B, PhQ_A^- would represent the most stable state in the PsaA-F689N mutant PSI, and to a smaller extent in the case of WT PSI. The absence of the F_A and F_B clusters would thus further stabilize PhQ_A^-, if such a large change did not greatly affect the potentials of the other cofactors (57).

The core of the photosynthetic RC of heliobacteria is composed of a homodimer of the PshA polypeptide, and the soluble PshB polypeptide was originally thought to act analogously to PsaC (58). However, PshB appears to be weakly bound to the PshA homodimer (59) and the same is true of the PscB polypeptide of the chlorobial RC (60), suggesting that this is a general property of homodimeric type I RCs. Thus, the homodimeric ancestor of the type I RCs probably harbored an F_X cluster but lacked a tightly bound ferredoxin-like F_A/F_B-binding subunit. In this context, a mutation that sufficiently delayed PhQ_A^- oxidation would result in an RC with characteristics of both RC families, i.e., a quinone-reducing acceptor side in a system performing bidirectional ET. Based on the results obtained in this study, one could argue that this might be sufficient to confer a type II-like function on a type I RC. The first photochemical event would result in the formation of the analog of PhQ_A^- with a quantum yield close to one, and the second photochemical act would produce PhQ_B^- equally efficiently, as shown here. Subsequent ET from PhQ_B^- to PhQ_A^- via F_X would result in a double reduction of the quinone, to quinol, assuming that there existed a pathway for efficient protonation of the semiquinone and/or quinolate form(s). (We deliberately omit in this discussion the need to couple proton transfer to the reduction of the quinone, as well as issues regarding binding of the quinone and release of the quinol. These issues are undoubtedly important and deserve careful discussion, but this would go beyond the scope of this article.) In this respect, it is worth noting that PSI is capable of a double reduction of plastoquinone (which has a higher redox potential than PhQ) when it is bound in the PhQ site (44). Although this reaction occurs with low quantum efficiency in PSI (44), the same may not be true of the type I RCs of the anoxygenic phototrophs.

SUPPORTING MATERIAL

Supporting Materials and Methods, five figures, and one table are available at http://www.biophysj.org/biophysj/supplemental/S0006-3495(15)00070-3.

AUTHOR CONTRIBUTIONS

S.S., F.R., and K.E.R. designed the experiment. B.B. made the mutant and did all genetic work. K.R., F.R., and S.S. participated in data collection and analysis and wrote the manuscript.

ACKNOWLEDGMENTS

We acknowledge the involvement of Dr. A. Jasaitis in the initial stages of this study.

This work was supported by grants from the Department of Energy (DE-FG02-08ER15989 to K.R., for the initial creation and characterization of the PsaA-F689N mutant) and the National Science Foundation (MCB-1052573 for the use of this mutant to study the effect of PhQ_A^- on the directionality of ET within PSI). F.R. received financial support from the CNRS and the Initiative d'Excellence Program of the French state (DYNAMO, ANR-11-LABX-0011-01).

SUPPORTING CITATIONS

References (61–68) appear in the Supporting Material.

REFERENCES

1. Gobets, B., and R. van Grondelle. 2001. Energy transfer and trapping in photosystem I. *Biochim. Biophys. Acta.* 1507:80–99.
2. Croce, R., and H. van Amerongen. 2013. Light-harvesting in photosystem I. *Photosynth. Res.* 116:153–166.
3. Caffarri, S., T. Tibiletti, …, S. Santabarbara. 2014. A comparison between plant photosystem I and photosystem II architecture and functioning. *Curr. Protein Pept. Sci.* 15:296–331.
4. Jennings, R. C., G. Zucchelli, and S. Santabarbara. 2013. Photochemical trapping heterogeneity as a function of wavelength, in plant photosystem I (PSI-LHCI). *Biochim. Biophys. Acta.* 1827:779–785.
5. Galka, P., S. Santabarbara, …, S. Caffarri. 2012. Functional analyses of the plant photosystem I-light-harvesting complex II supercomplex reveal that light-harvesting complex II loosely bound to photosystem II is a very efficient antenna for photosystem I in state II. *Plant Cell.* 24:2963–2978.
6. Diner, B. A., and F. Rappaport. 2002. Structure, dynamics, and energetics of the primary photochemistry of photosystem II of oxygenic photosynthesis. *Annu. Rev. Plant Biol.* 53:551–580.
7. Santabarbara, S., P. Heathcote, and M. C. W. Evans. 2005. Modelling of the electron transfer reactions in Photosystem I by electron tunnelling theory: the phylloquinones bound to the PsaA and the PsaB reaction

center subunits of PSI are almost isoenergetic to the iron-sulfur cluster F_X. *Biochim. Biophys. Acta.* 1708:283–310.

8. Rappaport, F., B. A. Diner, and K. E. Redding. 2006. Optical measurements of secondary electron transfer in photosystem I. *In* Photosystem I: The Light-Driven Plastocyanin:Ferredoxin Oxidoreductase. J. H. Golbeck, editor. Kluwer Academic Publishers, Dordrecht, pp. 223–244.
9. Jordan, P., P. Fromme, …, N. Krauss. 2001. Three dimensional structure of cyanobacterial Photosystem I at 2.5 Å resolution. *Nature.* 411:909–917.
10. Ben–Shem, A., F. Frolow, and N. Nelson. 2003. Crystal structure of plant photosystem I. *Nature.* 426:630–635.
11. Deisenhofer, O., K. Epp, …, H. Michel. 1985. Structure of the protein subunits in the photosynthetic reaction center of Rhodopseudomonas viridis at 3Å resolution. *Nature.* 318:618–624.
12. Allen, J. P., G. Feher, …, R. Huber. 1986. Structural homology of reaction centers from Rhodopseudomonas sphaeroides and Rhodopseudomonas viridis as determined by x-ray diffraction. *Proc. Natl. Acad. Sci. USA.* 83:8589–8593.
13. Zouni, A., H. T. Witt, …, P. Orth. 2001. Crystal structure of photosystem II from Synechococcus elongatus at 3.8 Å resolution. *Nature.* 409:739–743.
14. Umena, Y., K. Kawakami, …, N. Kamiya. 2011. Crystal structure of oxygen-evolving photosystem II at a resolution of 1.9 Å. *Nature.* 473:55–60.
15. Brettel, K. 1997. Electron transfer and arrangement of the redox cofactors in photosystem I. *Biochim. Biophys. Acta.* 1318:322–373.
16. Melkozernov, A. N., and R. E. Blankenship. 2005. Structural and functional organization of the peripheral light-harvesting system in photosystem I. *Photosynth. Res.* 85:33–50.
17. Müller, M. G., J. Niklas, …, A. R. Holzwarth. 2003. Ultrafast transient absorption studies on Photosystem I reaction centers from Chlamydomonas reinhardtii. 1. A new interpretation of the energy trapping and early electron transfer stePSIn Photosystem I. *Biophys. J.* 85:3899–3922.
18. Müller, M. G., C. Slavov, …, A. R. Holzwarth. 2010. Independent initiation of primary electron transfer in the two branches of the photosystem I reaction center. *Proc. Natl. Acad. Sci. USA.* 107:4123–4128.
19. Srinivasan, N., and J. H. Golbeck. 2009. Protein-cofactor interactions in bioenergetic complexes: the role of the A_{1A} and A_{1B} phylloquinones in Photosystem I. *Biochim. Biophys. Acta.* 1787:1057–1088.
20. Redding, K. E., and A. van der Est. 2006. The directionality of electron transfer in photosystem I. *In* Photosystem I: The Plastocyanin:Ferredoxin Oxidoreductase in Photosynthesis. J. H. Golbeck, editor. Kluwer Academic Publishers, Dordrecht, pp. 413–437.
21. Santabarbara, S., L. Galuppini, and A. P. Casazza. 2010. Bidirectional electron transfer in the reaction centre of photosystem I. *J. Integr. Plant Biol.* 52:735–749.
22. Guergova-Kuras, M., B. Boudreaux, …, K. E. Redding. 2001. Evidence for two active branches for electron transfer in photosystem I. *Proc. Natl. Acad. Sci. USA.* 98:4437–4442.
23. Xu, W., P. Chitnis, …, J. H. Golbeck. 2003. Electron transfer in cyanobacterial photosystem I: II. Determination of forward electron transfer rates of site-directed mutants in a putative electron transfer pathway from A_0 through A_1 to F_X. *J. Biol. Chem.* 278:27876–27887.
24. Santabarbara, S., I. Kuprov, …, M. C. W. Evans. 2005. Bidirectional electron transfer in photosystem I: determination of two distances between P_{700}^+ and A_1^- in spin-correlated radical pairs. *Biochemistry.* 44:2119–2128.
25. Santabarbara, S., I. Kuprov, …, M. C. W. Evans. 2006. Analysis of the spin-polarized electron spin echo of the $[P_{700}^+A_1^-]$ radical pair of photosystem I indicates that both reaction center subunits are competent in electron transfer in cyanobacteria, green algae, and higher plants. *Biochemistry.* 45:7389–7403.
26. Berthold, T., E. D. von Gromoff, …, G. Kothe. 2012. Exploring the electron transfer pathways in photosystem I by high-time-resolution electron paramagnetic resonance: observation of the B-side radical pair P700(+)A1B(−) in whole cells of the deuterated green alga Chlamydomonas reinhardtii at cryogenic temperatures. *J. Am. Chem. Soc.* 134:5563–5576.
27. Santabarbara, S., I. Kuprov, …, M. C. W. Evans. 2010. Directionality of electron-transfer reactions in photosystem I of prokaryotes: universality of the bidirectional electron-transfer model. *J. Phys. Chem. B.* 114:15158–15171.
28. Byrdin, M., S. Santabarbara, …, F. Rappaport. 2006. Assignment of a kinetic component to electron transfer between iron-sulfur clusters F_X and $F_{A/B}$ of Photosystem I. *Biochim. Biophys. Acta.* 1757:1529–1538.
29. Ali, K., S. Santabarbara, P. Heathcote, M. C. W. Evans, and S. Purton. 2006. Bidirectional electron transfer in photosystem I: replacement of the symmetry-breaking tryptophan close to the PsaB-bound phylloquinone A_{1B} with a glycine residue alters the redox properties of A_{1B} and blocks forward electron transfer at cryogenic temperatures. *Biochim. Biophys. Acta.* 1757:1623–1633.
30. Santabarbara, S., A. Jasaitis, …, K. E. Redding. 2008. Additive effect of mutations affecting the rate of phylloquinone reoxidation and directionality of electron transfer within photosystem I. *Photochem. Photobiol.* 84:1381–1387.
31. Santabarbara, S., K. Reifschneider, …, K. E. Redding. 2010. Interquinone electron transfer in photosystem I as evidenced by altering the hydrogen bond strength to the phylloquinone(s). *J. Phys. Chem. B.* 114: 9300–9312.
32. Srinivasan, N., S. Santabarbara, …, J. H. Golbeck. 2011. Alteration of the H-bond to the A_{1A} phylloquinone in Photosystem I: influence on the kinetics and energetics of electron transfer. *J. Phys. Chem. B.* 115: 1751–1759.
33. Mula, S., M. D. McConnell, …, A. van der Est. 2012. Introduction of a hydrogen bond between phylloquinone PhQ_A and a threonine sidechain OH group in photosystem I. *J. Phys. Chem. B.* 116:14008–14016.
34. Cohen, R. O., G. Shen, …, D. Stehlik. 2004. Evidence for asymmetric electron transfer in cyanobacterial photosystem I: analysis of a methionine-to-leucine mutation of the ligand to the primary electron acceptor A_0. *Biochemistry.* 43:4741–4754.
35. Giera, W., K. Gibasiewicz, …, A. Webber. 2009. Electron transfer from A_0 to A_1 in Photosystem I from Chlamydomonas reinhardtii occurs in both the A and B branch with 25–30-ps lifetime. *Phys. Chem. Chem. Phys.* 11:5186–5191.
36. Baymann, F., M. Brugna, U. Muhlenhoff, and W. Nitschke. 2001. Daddy, where did (PS)I come from? *Biochim. Biophys. Acta.* 1507: 291–310.
37. Li, Y., M. G. Lucas, …, K. E. Redding. 2004. Mutation of the putative hydrogen-bond donor to P700 of Photosystem I. *Biochemistry.* 43: 12634–12647.
38. Redding, K., F. MacMillan, …, J.-D. Rochaix. 1998. A survey of conserved histidines in the photosystem I: methodology and analysis of the PsaB-H656L mutant. *In* Photosynthesis: Mechanisms and Effects, *Vol. 1*. G. Garab, editor. Kluwer Academic Publishers, Dordrecht, pp. 591–594.
39. Harris, E. H. 1989. The Chlamydomonas Sourcebook. A Comprehensive Guide to Biology and Laboratory Use. Academic Press, San Diego.
40. Béal, D., F. Rappaport, and P. Joliot. 1999. A new high-sensitivity 10-ns time-resolution spectrophotometric technique adapted to in vivo analysis of the photosynthetic apparatus. *Rev. Sci. Instrum.* 70: 202–207.
41. Santabarbara, S., K. E. Redding, and F. Rappaport. 2009. Temperature dependence of the reduction of P_{700}^+ by tightly bound plastocyanin in vivo. *Biochemistry.* 48:10457–10466.
42. Agalarov, R., and K. Brettel. 2003. Temperature dependence of biphasic forward electron transfer from the phylloquinone(s) A_1 in photosystem I: only the slower phase is activated. *Biochim. Biophys. Acta.* 1604:7–12.

43. Vos, M. H., and H. J. van Gorkom. 1988. Thermodynamics of electron transfer in Photosystem I studied by electric field-stimulated charge recombination. *Biochim. Biophys. Acta.* 934:293–302.

44. McConnell, M. D., J. B. Cowgill, …, K. E. Redding. 2011. Double reduction of plastoquinone to plastoquinol in photosystem I. *Biochemistry.* 50:11034–11046.

45. Iwaki, M., S. Kumazaki, …, S. Itoh. 1996. ΔG^0 dependence of the electron transfer rate in the photosynthetic reaction center of plant photosystem I: natural optimization of reaction between chlorophyll a A_0 and quinone. *J. Phys. Chem.* 100:10802–10809.

46. Munge, B., S. K. Das, …, J. F. Rusling. 2003. Electron transfer reactions of redox cofactors in spinach photosystem I reaction center protein in lipid films on electrodes. *J. Am. Chem. Soc.* 125:12457–12463.

47. Ishikita, H., and E. W. Knapp. 2003. Redox potential of quinones in both electron transfer branches of photosystem I. *J. Biol. Chem.* 278:52002–52011.

48. Karyagina, I., Y. Pushkar, …, J. H. Golbeck. 2007. Contributions of the protein environment to the midpoint potentials of the A_1 phylloquinones and the F_x iron-sulfur cluster in photosystem I. *Biochemistry.* 46:10804–10816.

49. Ptushenko, V. V., D. A. Cherepanov, L. I. Krishtalik, and A. Y. Semenov. 2008. Semi-continuum electrostatic calculations of redox potentials in photosystem I. *Photosynth. Res.* 97:55–74.

50. Moser, C. C., and P. L. Dutton. 1992. Engineering protein structure for electron transfer function in photosynthetic reaction centers. *Biochim. Biophys. Acta.* 1101:171–176.

51. Page, C. C., C. C. Moser, …, P. L. Dutton. 1999. Natural engineering principles of electron tunnelling in biological oxidation-reduction. *Nature.* 402:47–52.

52. Schlodder, E., K. Falkenberg, …, K. Brettel. 1998. Temperature dependence of forward and reverse electron transfer from A_1^-, the reduced secondary electron acceptor in photosystem I. *Biochemistry.* 37: 9466–9476.

53. Li, Y., A. van der Est, …, K. E. Redding. 2006. Directing electron transfer within Photosystem I by breaking H-bonds in the cofactor branches. *Proc. Natl. Acad. Sci. USA.* 103:2144–2149.

54. Gibasiewicz, K., A. Dobek, …, W. Leibl. 2001. Modulation of primary radical pair kinetics and energetics in photosystem II by the redox state of the quinone electron acceptor Q_A. *Biophys. J.* 80:1617–1630.

55. Rappaport, F., M. Guergova-Kuras, …, J. Lavergne. 2002. Kinetics and pathways of charge recombination in photosystem II. *Biochemistry.* 41:8518–8527.

56. Shelaev, I. V., F. E. Gostev, …, A. Y. Semenov. 2010. Femtosecond primary charge separation in Synechocystis sp. PCC 6803 photosystem I. *Biochim. Biophys. Acta.* 1797:1410–1420.

57. Ishikita, H., D. Stehlik, …, E. W. Knapp. 2006. Electrostatic influence of PsaC protein binding to the PsaA/PsaB heterodimer in photosystem I. *Biophys. J.* 90:1081–1089.

58. Heinnickel, M., G. Shen, and J. H. Golbeck. 2007. Identification and characterization of PshB, the dicluster ferredoxin that harbors the terminal electron acceptors F_A and F_B in Heliobacterium modesticaldum. *Biochemistry.* 46:2530–2536.

59. Romberger, S. P., and J. H. Golbeck. 2012. The F_X iron-sulfur cluster serves as the terminal bound electron acceptor in heliobacterial reaction centers. *Photosynth. Res.* 111:285–290.

60. Jagannathan, B., and J. H. Golbeck. 2008. Unifying principles in homodimeric type I photosynthetic reaction centers: properties of PscB and the F_A, F_B and F_X iron-sulfur clusters in green sulfur bacteria. *Biochim. Biophys. Acta.* 1777:1535–1544.

61. Marcus, R. A., and N. Sutin. 1985. Electron transfer in chemistry and biology. *Biochim. Biophys. Acta.* 811:265–322.

62. Hopfield, J. J. 1974. Electron transfer between biological molecules by thermally activated tunnelling. *Proc. Natl. Acad. Sci. USA.* 71:3640–3644.

63. Devault, D. 1980. Quantum Mechanical Tunnelling in Biological Systems. Cambridge University Press, Cambridge.

64. Jortner, J. 1976. Temperature dependent activation energy for electron transfer between biological molecules. *J. Chem. Phys.* 64:4860–4868.

65. Giera, W., V. M. Ramesh, …, K. Gibasiewicz. 2010. Effect of the P_{700} pre-oxidation and point mutations near A_0 on the reversibility of the primary charge separation in Photosystem I from Chlamydomonas reinhardtii. *Biochim. Biophys. Acta.* 1797:106–112.

66. Lefebvre-Legendre, L., F. Rappaport, …, J. D. Rochaix. 2007. Loss of phylloquinone in Chlamydomonas affects plastoquinone pool size and photosystem II synthesis. *J. Biol. Chem.* 282:13250–13263.

67. Hervás, M., J. A. Navarro, and M. A. De La Rosa. 2003. Electron transfer between membrane complexes and soluble proteins in photosynthesis. *Acc. Chem. Res.* 36:798–805.

68. Hope, A. B. 2000. Electron transfers amongst cytochrome f, plastocyanin and photosystem I: kinetics and mechanisms. *Biochim. Biophys. Acta.* 1456:5–26.

Controlling electron transfer between the two cofactor chains of Photosystem I by the redox state of one of their components.

Stefano Santabarbara[†‡§], Bradford Bullock[¶], Fabrice Rappaport[‡*], Kevin Redding[†*]

[†]Department of Chemistry & Biochemistry, Arizona State University, 1711 S. Rural Rd., Tempe, Arizona 85287, U.S.A. [‡]Institut de Biologie Physico-Chimique, UMR7141 CNRS-UPMC, 13 Rue Pierre et Marie Curie, 75005, Paris, France [§]Istituto di Biofisica, Consiglio Nazionale delle Ricerche, Via Celoria 26, 20133 Milano, Italy. [¶]Dept. Chemistry, University of Alabama, 206 Shelby Hall, 250 Hackberry Lane, Tuscaloosa, AL 35487-0336

Supporting Material

i) Modeling of secondary electron transfer reactions in the RC of PSI

The kinetics of secondary electron transfer reactions reaction in PSI has been modeled, as previously described in detail (1, 2), by solving a system of linear differential equations that consider explicitly three states, PhQ_A^-, PhQ_B^- and F_X^-. The rate constant associated with each ET event was determined according to Marcus theory of electron transfer, in the "high-temperature approximation" that does not explicitly consider coupling with the nuclear modes (3–4):

$$k_{et} = \frac{2\pi}{\mathrm{h}} \frac{\left|H_{DA}\right|_0^2 e^{-\beta X_{DA}}}{\sqrt{4\pi\lambda_{tot} k_b T}} e^{-\frac{(\Delta G^0 + \lambda_{tot})^2}{4 k_b T \lambda_{tot}}} \qquad \text{Equation S1}$$

For the maximal value of the electron coupling factor, $\left|H_{DA}\right|_0^2$, we consider a value of ~1.5 x10^{-3} eV^2 (e.g. 5 – 6), attenuated exponentially by a factor β = 1.3 – 1.4 $Å^{-1}$ (7, 8) weighted for donor-acceptor distance X_{DA}, taken from the PSI structure from *T. elongatus* (9, PDB ID: 1JB0). The remaining parameters in the simulations are the (total) reorganization energy (λ_{tot}) and the standard Gibbs free energy difference ΔG^0. In order to limit the number of variables, the value of λ_{tot} has been

initially taken to be equal for all the reactions considered (λ_{tot}=0.7 eV). This value lies in the middle of the reported spread for ET within proteins (7, 8), and is similar to values obtained from the analysis of experimental data (10 – 12) and kinetic modeling (1, 2) of PhQ^- oxidation reactions. Therefore, only the ΔG^0 values need to be adjusted to describe qualitatively the experimental results. Since the model considers explicitly three states, the decay is described by three exponential lifetimes (and three associated amplitudes). Two of the lifetimes fall in the 5–30 ns interval and are considered to describe collectively the fastest phase of PhQ^- oxidation, whereas the remaining one describes the slowest phase observed experimentally (1, 2).

As previously discussed (1, 2, 13, 14), it is possible to obtain a good *qualitative* agreement between the experimental results and the simulations considering that $\Delta G^0_{PhQ_A^- \rightarrow F_X} > 0$ and $\Delta G^0_{PhQ_B^- \rightarrow F_X} < 0$, (i.e., oxidation of PhQ_A^- is slightly endergonic, with a value of ~1–2 k_bT). Although the numerous approximations implicitly made in the model prevent going beyond a qualitative description of the ET kinetics, it has yielded a rather good agreement between simulated and experimental lifetimes and amplitudes of the slow and fast PhQ^- oxidation phases (1, 2, 13, 14). The most relevant parameters to model the wild-type kinetics are reported in Table S1.

In order to simulate the kinetics in PsaA-F689N with minimal perturbation of the WT parameters, the midpoint potential of the PhQ_A/PhQ_A^- couple needs to be downshifted by 125 mV (thereby $\Delta G^0_{PhQ_A^- \rightarrow F_X}$ = 135 meV ~ $5\,k_bT$), so that this reaction is rather unfavorable, even when coupled with the very favorable oxidation of F_X^- ($\Delta G^0_{F_X^- \rightarrow F_{A/B}}$ < –150 meV). This yields a relatively good description of the lifetimes measured experimentally, including the extremely slow 17-μs component, as well as the faster decay of the rapid PhQ^- oxidation phase (Table S1). However, the amplitude associated with the slow 17-μs component is predicted by the simulation to be significantly larger than was seen experimentally (Fig. S1 and Table S1). A possible explanation for this discrepancy is that the mutation changes parameters besides the midpoint potential of PhQ_A/PhQ_A^-, such as modification of the reorganization energy (λ_{tot}) or the nuclear mode coupled to the ET reactions ($\bar{\omega}$).

This would not be unprecedented, since it was necessary to consider changes both in ΔG^0 as well as in $\bar{\omega}$ to explain the temperature-dependence of the kinetics in the PsaA-L722T mutant of *C. reinhardtii* (15). As the nuclear modes are not treated explicitly, due to the high-temperature approximation in our model, we altered the value of λ_{tot} to obtain a closer match between the simulations and experimental results. Raising the value of $\lambda_{tot,\mathrm{PhQ_A^-}\rightarrow\mathrm{F_X}}$ from 0.7 to 1 eV and that of $\Delta G^0_{\mathrm{PhQ_A^-}\rightarrow\mathrm{F_X}}$ from 10 meV to 115 meV in PsaA-F689N yields lifetimes that match experimental values well (Table S1). Importantly, the amplitude ratio of the slow:fast PhQ^- phases is now predicted to be ~0.80:0.20 in the mutant, which agrees well with the value estimated from the data (0.75:0.25, averaged over the near-UV PhQ^- absorption band).

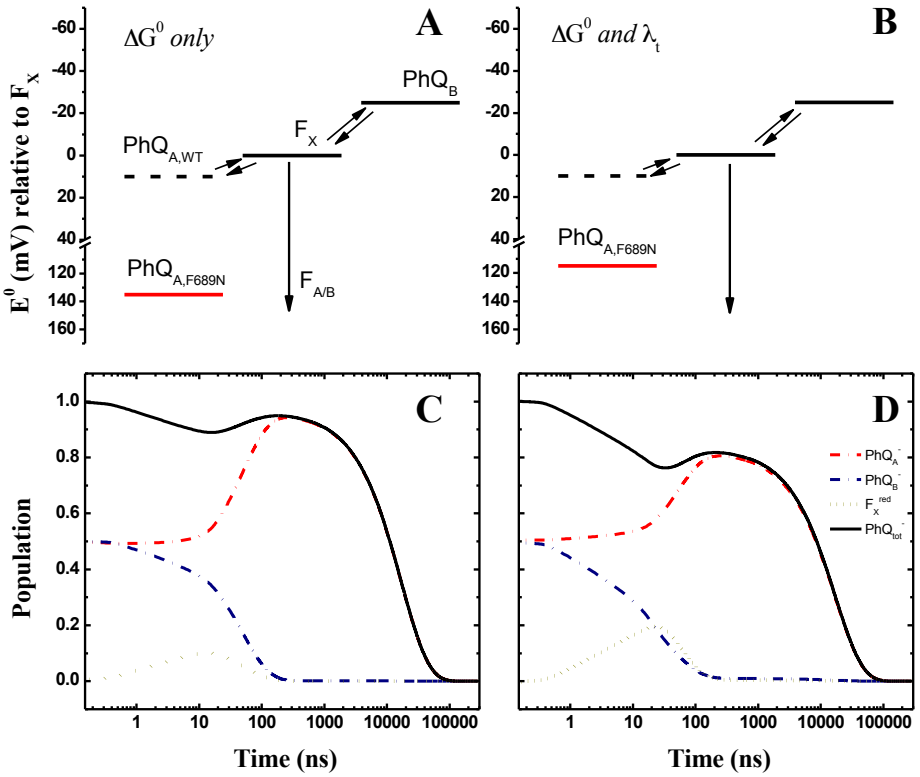

Figure S1. Simulations of ET kinetics in the PsaA-F689N mutant: energetics of the system (**A, B**) and calculated population evolutions (**C, D**). **Panels A** and **C** depict the situation obtained when modifying *only* the redox potential of $\mathrm{PhQ_A}/\mathrm{PhQ_A^-}$, and hence the free energy difference for the oxidation reaction in the mutant with respect to the wild type. **Panels B** and **D** display the simulation with alterations of both the standard free energy change and the reorganization energy of $\mathrm{PhQ_A^-}$ oxidation. Population evolution of $\mathrm{PhQ_A^-}$ (red dash-dotted lines), $\mathrm{PhQ_B^-}$ (blue dash-dotted lines) and $\mathrm{F_X}$

(golden dotted lines) derived from the modeling are shown. The solid black line depicts the "total" population evolution of PhQ^- (i.e., $PhQ_A^- + PhQ_B^-$).

Table S1. Values of the parameters used to simulate ET reactions in PS I.

	Input Parameters			Simulation Outputs				
	ΔG^0 (meV)	λ_{tot} (meV)	k_i^{-1} (ns)	τ_i (ns)	$A_{i,\,PhQ_A}$	$A_{i,\,PhQ_B}$	$A_{i,\,F_X}$	$A_{i,\,PhQ_{A+B}}$
Wild Type								
$PhQ_A^- \rightarrow F_X$	+10	700	33	9.2	0.21	0.18	-0.44	0.39
$PhQ_B^- \rightarrow F_X$	-25	700	18	23.1	-0.27	0.19	0.12	-0.09
				261.5	0.56	0.13	0.32	0.70
PsaA-F689N								
$PhQ_A^- \rightarrow F_X$	+135	700	993	4.2	0.13	0.02	-0.15	0.15
$PhQ_B^- \rightarrow F_X$	-25	700	18	48.0	-0.59	0.48	0.15	-0.11
				17000	0.96	0.002	0.005	0.96
$PhQ_A^- \rightarrow F_X$	+115	1000	6130	11	0.095	0.25	-0.41	0.35
$PhQ_B^- \rightarrow F_X$	-25	700	18	48	-0.41	0.24	0.40	-0.16
				17000	0.82	0.01	0.004	0.81

Parameters used to simulate PhQ^- oxidation in WT and the PsaA-F689N mutants of *C. reinhardtii* and results of the simulations in terms of lifetimes (τ_i) and amplitudes (A_i). $A_{i,\,PhQ_{A+B}} \equiv A_{i,\,PhQ_A} + A_{i,\,PhQ_B}$ for each τ_i. Simulations were performed altering either only the value of $\Delta G^0_{PhQ_A^- \rightarrow F_X}$ or both $\Delta G^0_{PhQ_A^- \rightarrow F_X}$ and $\lambda_{tot,PhQ_A^- \rightarrow F_X}$. The parameters used to model the oxidation of reduced F_X were held fixed for all simulations and corresponded to $\Delta G^0_{F_X^r \rightarrow F_A}$ = -155 meV and $\lambda_{tot,F_X^r \rightarrow F_A}$ = 700 meV. The temperature in all simulations was 298 K. Initial conditions were: $PhQ_A^- = PhQ_B^- = 0.5;\ F_X = 0$.

ii) Analysis of pump-pump-probe kinetics.

Figure S2 shows a comparison of the pump-probe and the pump-pump probe kinetics at 445 nm. This wavelength was selected as a marker for $[P_{700}^{+}A_0^{-}]$ charge recombination, since the bleaching due to A_0^{-} is still significant at this wavelength, while the contributions of P_{700}^{+} and electrochromic shifts of nearby pigments are much less significant (16–18). The comparison of these two experiments shows negligible differences for the WT on the short time scale (<200 ns, when charge recombination is expected to occur (16–18)), whereas some difference occurs on the longer time scale dominated by P_{700}^{+} reduction. This is due to the fact that there is less pre-bound plastocyanin available after the second flash, when it is close to the first flash, causing the reduction of P_{700}^{+} to be overall slower (i.e., there is a shift in the amplitudes of the ~6-μs and ~60-μs components towards the latter). A similar difference in the long time scale is observed for the PsaA-F689N mutant. In addition, a slight difference is observed on the short time scale, the relative magnitude of which is comparable to that observed at 395 nm (see Figure 3B of the main body). However, it is much smaller, since the absorption difference at 445 nm is much smaller than at 395 nm in the $[PhQ^{-} - PhQ]$ difference spectrum (see Figure 2 of the main body).

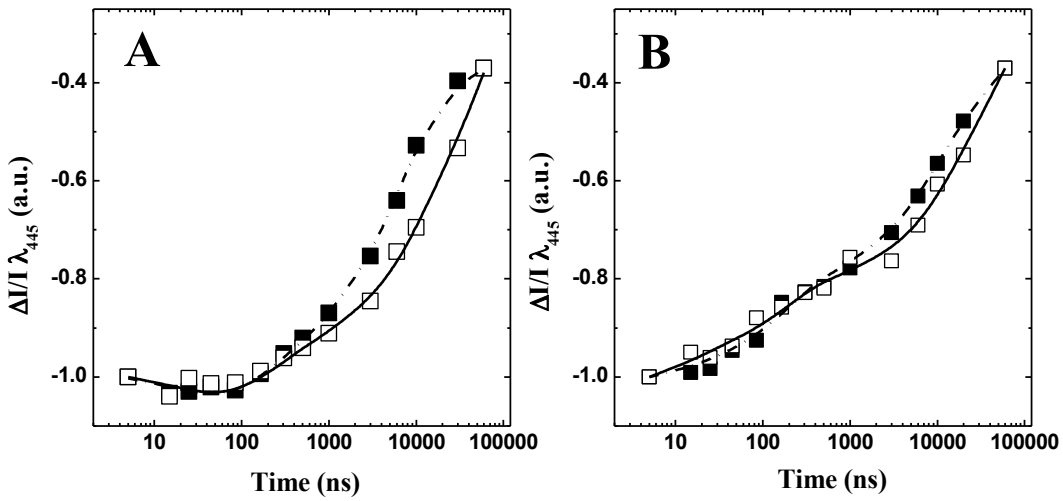

Figure S2. Comparison of kinetics monitored at 455 nm by pump-probe and pump-pump-probe (ΔT=15 μs) experiments in the WT (**A**) and the PsaA-F689N (**B**) strains. The open symbols and solid lines are the experimental data and fits of pump-pump-probe experiments, respectively, whereas the closed symbols and the dashed lines are the pump-probe kinetics acquired on the same sample using the pump-pump-probe set-up with the first pump pulse shuttered.

iii) Simulations of pump-pump-probe experiments

In the pump-pump-probe experiment reported in this study, the first pump pulse "prepares" the system in a given redox state of the cofactors in the reaction center. PSI can be present in four distinct "redox states" at the moment the second pump pulse is delivered to the sample at given delay time (ΔT) after the first actinic flash. Those are denoted as i) $\sigma_{P_{700}^{+}PhQ^{-}}$, the fraction in which the primary donor (P_{700}) is oxidized and the secondary acceptor (PhQ_A) is reduced; ii) $\sigma_{P_{700}^{+}PhQ^{-}}$ the fraction in which both P_{700} and PhQ_A are oxidized; iii) $\sigma_{P_{700}PhQ}$, the fraction in which P_{700} is reduced and PhQ_A is oxidized; iv) $\sigma_{P_{700}PhQ^{-}}$ the fraction in which both P_{700} and PhQ_A are reduced. The fractional populations of these four redox states, at any pump-pump delay ΔT, is the combinatorial probability of the normalized population evolution of $P_{700}^{(+)}$ and $PhQ_A^{(-)}$ that are determined from the classic pump-probe experiment. Figure S3 shows the calculated populations of the four different redox states, as a function of ΔT, for the wild-type and the PsaA-F689N mutant scenarios.

We now turn to consider how each of these redox states of the RC would evolve following the second actinic excitation in the pump-pump-probe experiment. We make the simple assumption that when the electron donor is oxidized (i.e. P_{700}^{+}) the system cannot undergo charge separation (i.e. it is "closed"). Therefore, fractions $\sigma_{P_{700}^{+}PhQ^{-}}$ and $\sigma_{P_{700}^{+}PhQ}$ would not contribute to the light-induced signal. We note that P_{700} may not be the primary electron donor (1, 19–21), and that initial charge separated state might be $[ec2_A^{+}ec3_A^{-}]$ instead. While the latter could be populated even in the presence of P_{700}^{+}, it has been shown in this case that charge recombination of the initial radical pair takes place in the sub-ns time range (22) and would therefore not contribute to the monitored transient absorption in our experiment. Therefore, the second pump pulse is assumed to be ineffective in PSI with P_{700}^{+}.

In the $\sigma_{P_{700}PhQ}$ fraction of centers, the system is simply reset and the evolution of the state produced by second pump flash should be the same as with a single flash. We can model this with by assuming that PSI RCs in this fraction will behave identically to those in the simple pump-probe experiment.

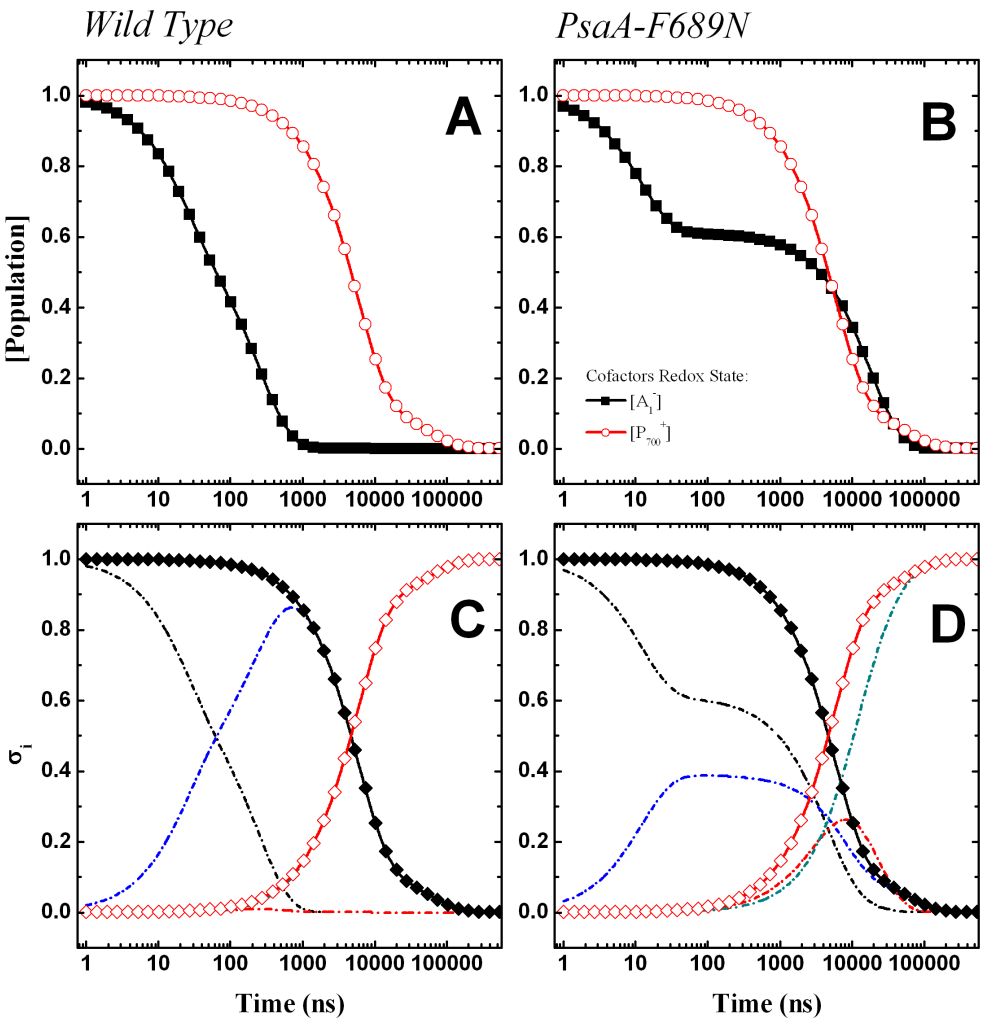

Figure S3. Comparison of the population evolution of P_{700}^{+} (open red symbols) and PhQ^{-} (solid black symbols) derived from the fits of the experimental data for the wild type (**A**) and the PsaA-F689N mutant (**B**). Note that both the "fast" and "slow" phases of P_{700}^{+} reduction and of PhQ^{-} oxidation have been included in the calculation. Probabilities of the different "redox states" of the system $\sigma_{P_{700}^{+/0}PhQ^{-/0}}$ calculated from the population evolution of the wild type (**C**) and the PsaA-F689N mutant (**D**): $\sigma_{P_{700}^{+}PhQ^{-}}$: dash-dotted black lines, $\sigma_{P_{700}^{+}PhQ}$: dash-dotted blue lines, $\sigma_{P_{700}PhQ^{-}}$: dash-dotted red lines, $\sigma_{P_{700}PhQ}$: dash-dotted green lines (not discernable in WT due to overlap with red line). Also shown are probabilities of PSI centers being "closed" ($\sigma_{closed} = \sigma_{P_{700}^{+}PhQ} + \sigma_{P_{700}^{+}PhQ^{-}}$: solid black diamonds) or "open" ($\sigma_{open} = \sigma_{P_{700}PhQ} + \sigma_{P_{700}PhQ^{-}}$: open red diamond).

The most interesting case is when both the electron donor and electron acceptor are reduced ($\sigma_{P_{700}PhQ^{-}}$). Under these conditions charge separation is initiated

in the presence of a charged molecule (PhQ_A^-) in close proximity to one of the cofactors involved in charge separation and this may have several consequences:

i) It may accelerate charge recombination of the initial radical pair formed after the second flash, thereby decreasing the overall yield of "long lived" P_{700}^+ (i.e., >5 ns, and thus detectable by our set-up).

ii) A second light-induced electron transfer in ETC_A may lead to the double reduction of PhQ_A. Because the quinol is stable and unavailable as an electron acceptor, its presence would promote $P_{700}^+ec3_A^-$ charge recombination. The signature of such a process would also be a decrease of long-lived P_{700}^+, as previously shown for a mutation in the PhQ biosynthetic pathway that leads to substitution of PhQ by plastoquinone in PSI; reduction of the introduced quinone to a quinol resulted in the decay of P_{700}^+ in the tens of ns (**23, 24**).

iii) The presence of PhQ_A^- may modify the energetics of charge separation in ETC_A by Coulombic interaction, making it more likely for charge separation to occur in ETC_B.

Based on these considerations, it is possible to describe the kinetics observed in pump-pump-probe experiments by the combination of three exponential decay functions $f^{pp}(t,\lambda) = \sum_{u=1}^{3} f_u^{pp}(t,\lambda)$ where:

$$f_1^{pp}(t,\lambda) = (\sigma_{P_{700}^+PhQ^-} + \sigma_{P_{700}^+PhQ}) \cdot (\sum_{i=1}^{n} A_i(\lambda) \cdot e^{-(\frac{t+\Delta t}{\tau_i})} + A_\infty(\lambda))$$

$$f_2^{pp}(t,\lambda) = (\sigma_{P_{700}PhQ}) \cdot (\sum_{i=1}^{n} A_i(\lambda) \cdot e^{-(\frac{t}{\tau_i})} + A_\infty(\lambda)) \qquad \text{Equation S2.}$$

$$f_3^{pp}(t,\lambda) = (\sigma_{P_{700}PhQ^-}) \cdot (\sum_{j=1}^{n} A_j(\lambda) \cdot e^{-(\frac{t}{\tau_j})} + A_\infty(\lambda))$$

As shown in Figure S3, the fraction of center $\sigma_{P_{700}PhQ^-}$ is significant only in the PsaA-F689N mutant. Hence, in the wild-type, the pump-pump-probe experiment only depends on $f_1^{pp} + f_2^{pp}$ (as described in Equation S2), so that the experimental results

can be described from the results of the standard pump-probe experiments alone. We note that, as shown in Figure 1, a residual difference absorption signal is observed at delay times longer than 100 μs. This is due to several processes occurring in the thylakoid membranes of whole *C. reinhardtii* cells (*e.g.* transmembrane electric field decay, cytochrome *f* redox changes). These processes, however, take place much later than ET events within the reaction centers and they are thus treated as a non-decaying component in the data fit (see Figure 1 of the main body). As a starting point, we assumed that the relative amplitude of the non-decaying fraction would scale linearly with the fraction of photochemically active PSI RCs. The simulations made according to this model, taking the parameters from the fits of the pump-probe experiment, are shown in Figure S4. The pump-pump-probe kinetics is described adequately for the sub-μs decay window by this model. However, the simulations failed to describe precisely the P_{700}^{+} reduction contribution. By allowing the amplitude of these "late" phases associated with P_{700}^{+} reduction to vary (without changing the lifetimes or amplitudes associated with PhQ^{-} oxidation), the agreement became excellent (Fig. S4). Changes in the decays in the μs time window are likely associated with a shift in the ratios of bound/unbound and/or oxidized/reduced plastocyanin at the time the second excitation pulse hits the RC. Since the relative amplitudes of the "fast" (~6 μs) and "slow" (~56 μs) reduction phases of P_{700}^{+} are related to the formation of the PSI-plastocyanin binary complex, and the slow phase, which is limited by dissociation/association of plastocyanin (e.g. **25, 26**), is comparable to the values of ΔT used in this study, a redistribution of the P_{700}^{+} reduction phases is expected. The simulations also show the relative contributions of signal arising from different initial redox states at ΔT, where it can be appreciated that the dominant contribution in the WT is $\sigma_{P_{700}PhQ}$ (dashed blue line) and that $\sigma_{P_{700}PhQ^{-}}$ (dashed magenta line) is completely negligible.

In contrast, the $\sigma_{P_{700}PhQ^{-}}$ fraction becomes significant in PsaA-F689N (Fig. S3). One of the possible scenarios when charge separation takes place in the presence of PhQ_A^{-} is that it is biased to occur preferentially on ETC_B, due to inhibition of primary radical pair formation, as the electron acceptor is located next to the PhQ_A^{-} anion. The simplest case that one can consider is that, in the presence of PhQ_A^{-}

i) no charge recombination occurs on ETC_A;

ii) no charge separation occurs down ETC_A and the electrons are all redirected down ETC_B; and

iii) the rates of the electron transfer reactions down ETC_B are unaffected by the presence of PhQ_A^-.

Point (iii) is an approximation because the kinetics of PhQ_B^- oxidation may be influenced by the presence of PhQ_A^- and F_X^- (see section 1 of the Supplementary material). However, since the dominating lifetime describing PhQ_B^- approaches the value of the inverse of kinetic rate constant associated to the $PhQ_B^- \rightarrow F_X$ event, this approximation appears to be reasonable, especially since the simulations are meant to provide only a semi-qualitative description of the pump-pump-probe experiments.

The results of the simulation made under these assumptions are also shown in Figure S4. It can be seen that they nicely fit the experimental results, but for a slight difference in offset that, when allowed to change freely, yields a very satisfactory description of the data. As in the case of the WT, the change in offset is likely due to changes in the fast:slow P_{700}^+ reduction phases by plastocyanin, which in the PsaA-F689N mutant strain are partially overlapped by the 17-µs PhQ^- oxidation component and are therefore less obvious. This bears little consequence for the interpretation of the transient absorption in the sub-µs time window, which is the central issue dealt with in this study.

One of the critical advantages of these simulations is that it allows one to discriminate the contributions of the different populations to the decay observed after the second excitation (Fig. S4 panels B and D). In the WT, the contribution of $\sigma_{P_{700}PhQ^-}$ is essentially nonexistent, and the closed fractions cause an offset. Thus all of the kinetics are due to the $\sigma_{P_{700}PhQ}$ fraction, as predicted. The tail of decay elicited by the first actinic pulse in the closed fraction (i.e., $\sigma_{P_{700}^+PhQ^-}$; Fig. S4D, grey dashed line) has a much stronger contribution in the PsaA-F689N mutant, due to the slower oxidation of PhQ_A^-. This fraction and the $\sigma_{P_{700}PhQ}$ fraction (dashed blue line) together account for nearly all of the decay at 395 nm in the µs timescale in the mutant. Thus, nearly all of the decay at 395 nm in the $\sigma_{P_{700}PhQ^-}$ fraction (dash-dotted magenta line)

occurs in <100 ns and can be attributed to oxidation of PhQ_B^-. Therefore, within the confidence margin of the fits, it can be concluded that charge separation is biased towards ETC_B with a yield close to unity when PhQ_A^- is present in the system.

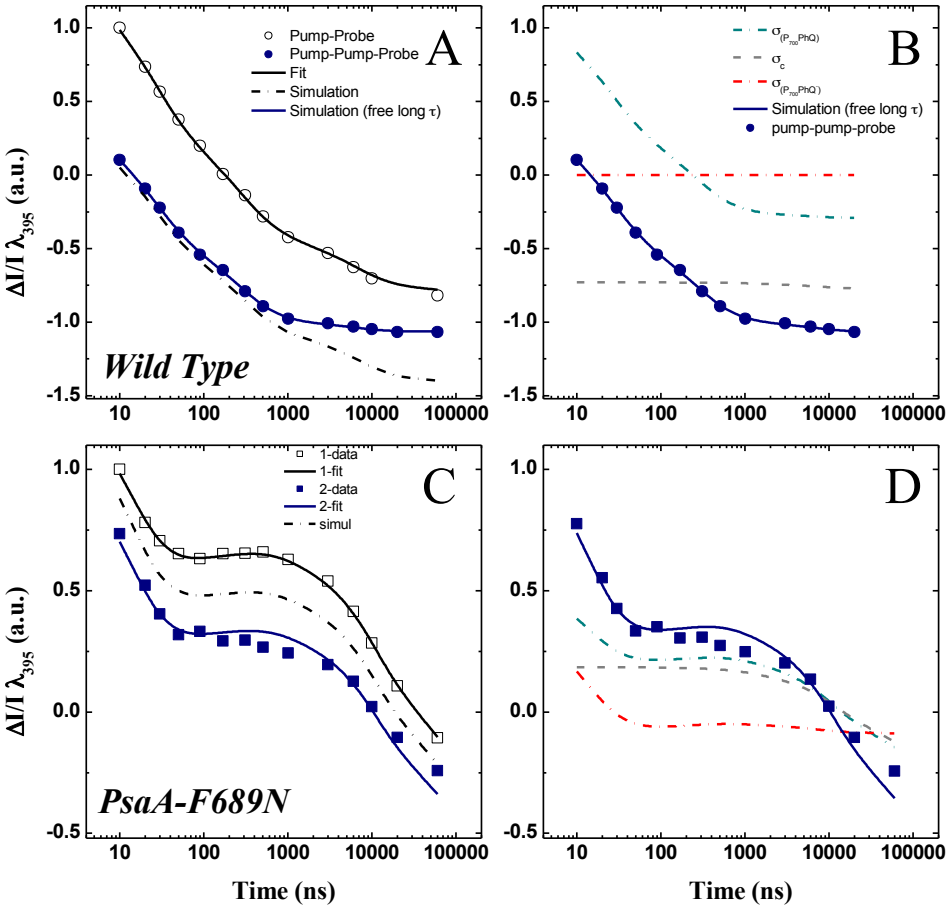

Figure S4. Comparison of experimental results and simulation of pump-pump-probe kinetics in the wild type (**A, B:** blue circles) and the PsaA-F689N strain (**C, D:** blue squares), monitored at 395 nm using $\Delta T = 15$ µs. The simulations are based on the fit of the pump-probe data, which are also shown for the WT (**A:** open circles) and the PsaA-F689N (**C:** open squares). The simulations according to Equation S3 are shown as black dash-dotted lines. The solid blue lines represent a mixed fit-simulation in which only the offset ($A_\infty(\lambda)$) is allowed to vary (PsaA-F689N) or the offset and the relative amplitudes of P_{700}^+ reduction (wild-type). Panels **B** and **D** show the de-convolution of the contributions to the pump-pump-probe absorption difference, for the case of WT (**B**) and the PsaA-F689N mutant (**D**) strains. Shown are the contributions of the signal arising from the different fractions after the second pump pulse: $\sigma_{P_{700}PhQ^-}$ (dash-dotted red line); $\sigma_{P_{700}PhQ}$ (dash-dotted green line); σ_{closed} (dashed grey line).

To further test this model, we have simulated the signal dependence as a function of the pump-pump delay time (Fig. S5), where the parameters related to the signal amplitude and the contribution of the "fast phase" have been calculated as for the experimental results. Both parameters are simulated satisfactorily. The fit to the simulations in terms of the exponential decays yields values τ_A=15 µs and τ_B=12 µs (7 µs and 55 µs for a bi-exponential recovery) which are very close to that obtained from the measurements (Figure 4, main body).

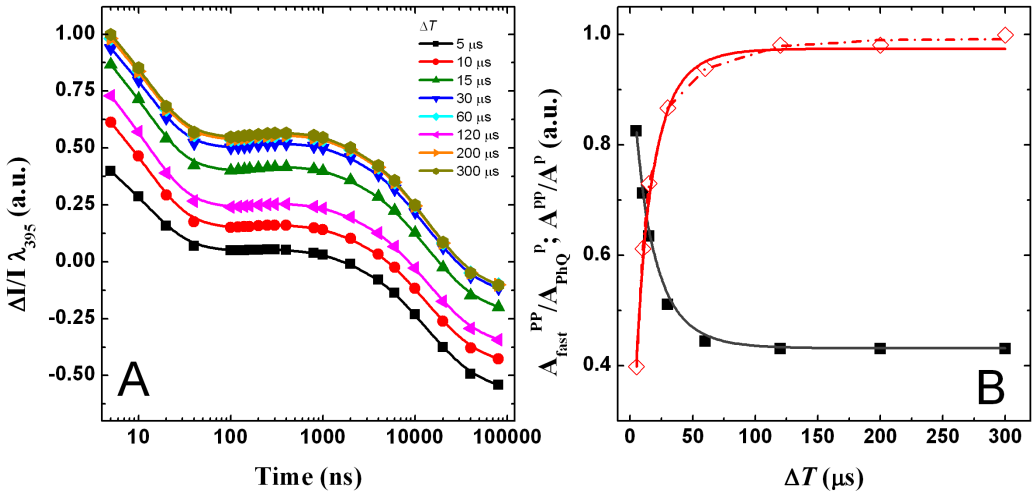

Figure S5. Panel A: Simulation of pump-pump-probe kinetics (at 395 nm) using different pump-pump delays (ΔT) ranging from 5 to 300 µs in the PsaA-F689N mutant strain. **Panel B:** Recovery of the difference absorption signal (A_0^{PP}/A_0^{P}) as a function of ΔT (red diamonds), and fractional contribution of the fast decay phase ($A_{fast}^{PP}=A_{40ns}^{PP} - A_0^{PP}$) to the difference absorption detected in the pump-pump-probe measurements (solid squares), calculated from the simulated kinetics shown in Panel **A**. The lines are fits to the estimated parameter using a single exponential (solid) or biexponential (dash-dotted) decay. The best fit for the initial amplitude recovery is obtained considering a biexponential relaxation ($\tau_{B,1}$= 7 µs and $\tau_{B,2}$=55 µs), whereas the decrease of the fractional amplitude of A_{fast}^{PP} as a function of ΔT is satisfactorily described by a single exponential (τ_A =15 µs).

It is thus possible to conclude that the presence of a meta-stable intermediate, such as PhQ_A^-, affects the primary photochemical process so that a *stable* charge separated state is formed only on ETC_B, resulting in reduction of PhQ_B. Hence, PSI essentially performs what could be considered a unidirectional (or extremely

asymmetric) ET as a result of the marked redistribution of the probability of utilization of the two active ET branches caused by the semiquinone anion in the A-branch.

Supporting References

1. Santabarbara, S., P. Heathcote, and M.C.W. Evans. 2005. Modelling of the electron transfer reactions in Photosystem I by electron tunnelling theory: the phylloquinones bound to the PsaA and the PsaB reaction centre subunits of PS I are almost isoenergetic to the iron–sulfur cluster F_X. Biochim. Biophys. Acta – Bioenergetics. 1708:283–310.

2. Santabarbara, S., L. Galuppini, and A.P. Casazza. 2010. Bidirectional electron transfer in the reaction centre of photosystem I. J. Integr. Plant. Biol. 52: 735–749.

3. Marcus, R.A., and N. Sutin 1985. Electron transfer in chemistry and biology. Biochim. Biophys. Acta. 811:265–322.

4. Hopfield, J.J. 1974. Electron transfer between biological molecules by thermally activated tunnelling. Proc. Natl. Acad. Sci. USA. 71:3640–3644.

5. Devault, D. 1980. Quantum mechanical tunnelling in biological systems. Cambridge University Press.

6. Jortner, J. 1976. Temperature Dependent Activation Energy for Electron Transfer Between Biological Molecules. J. Chem. Phys. 64:4860–4868.

7. Moser, C.C., and P.L. Dutton. 1992. Engineering protein structure for electron transfer function in photosynthetic reaction centers. Biochim. Biophys. Acta. 1101:171–176.

8. Page, C.C., C.C. Moser, X. Chen, and P.L. Dutton. 1999. Natural engineering principles of electron tunnelling in biological oxidation-reduction. Nature. 402:47–52

9. Jordan, P., P. Fromme, H.T. Witt, O. Klukas, W. Saenger, and Krauss N (2001) Three dimensional structure of cyanobacterial Photosystem I at 2.5 Å resolution. Nature. 411:909–917.

10. Agalarov R. and K. Brettel. 2003. Temperature dependence of biphasic forward electron transfer from the phylloquinone(s) A_1 in photosystem I: only the slower phase is activated. Biochim. Biophys. Acta – Bioenergetics. 1604:7–12.

11. Schlodder, E., K. Falkenberg, M Gergeleit, and K. Brettel. 1998. Temperature dependence of forward and reverse electron transfer from A_1^-, the reduced secondary electron acceptor in photosystem I. Biochemistry. 37:9466–9476

12. Santabarbara, S., K.E. Redding, and F. Rappaport. 2009. Temperature dependence of the reduction of P_{700}^+ by tightly bound plastocyanin in vivo. Biochemistry. 48:10457–10466.

13. Ali, K., S. Santabarbara, P. Heathcote, M.C.W. Evans, and S. Purton. 2006. Bidirectional electron transfer in photosystem I: replacement of the symmetry–breaking tryptophan close to the PsaB–bound phylloquinone A_{1B} with a glycine residue alters the redox properties of A_{1B} and blocks forward electron transfer at cryogenic temperatures. Biochim. Biophys. Acta – Bioenergetics. 1757:1623–1633.

14. Santabarbara, S., K. Reifschneider, A. Jasaitis, F. Gu, G. Agostini, D. Carbonera, F. Rappaport, and K.E. Redding. 2010. Interquinone electron transfer in photosystem I as evidenced by altering the hydrogen bond strength to the phylloquinone(s). J. Phys. Chem. B. 114:9300–9312.

15. Mula, S., M.D. McConnell, A Ching, N. Zhao N, H.L. Gordon, G. Hastings, K.E. Redding, and A. van der Est. 2012. Introduction of a hydrogen bond between phylloquinone PhQ_A and a threonine side-chain OH group in photosystem I. J. Phys. Chem. B. 116:14008–14016.

16. Brettel, K. 1997. Electron transfer and arrangement of the redox cofactor in photosystem I. Biochim. Biophys. Acta – Bionergetics. 1318:322–373.

17. Vos, M.H. and H.J. van Gorkom. 1988. Thermodynamics of electron transfer in Photosystem I studied by electric field-stimulated charge recombination. Biochim. Biophys. Acta – Bioenergetics. 934:293–302.

18. Byrdin, M., S. Santabarbara, F. Gu, W.V. Fairclough, P. Heathcote, K.E. Redding and F. Rappaport. 2006. Assignment of a kinetic component to electron transfer between iron-sulfur clusters F_X and $F_{A/B}$ of Photosystem I. Biochim. Biophys. Acta – Bioenergetics. 1757:1529–1538.

19. Müller, M.G., J. Niklas, W. Lubitz, and A.R. Holzwarth. 2003. Ultrafast transient absorption studies on Photosystem I reaction centers from Chlamydomonas reinhardtii. 1. A new interpretation of the energy trapping and early electron transfer stePSIn Photosystem I. Biophys. J. 85:3899–3922.

20. Müller, M.G., C. Slavov, R. Luthra, K.E. Redding, and A.R. Holzwarth. 2010. Independent initiation of primary electron transfer in the two branches of the photosystem I reaction center. Proc. Natl. Acad. Sci. USA. 107:4123–4128.

21. Li, Y., A. van der Est, M.G. Lucas, V.M. Ramesh, F. Gu, A. Petrenko, S. Lin, A.N. Webber, F Rappaport, and K.E. Redding. 2006. Directing electron transfer within Photosystem I by breaking H-bonds in the cofactor branches. Proc. Natl. Acad. Sci. USA. 103:2144–2149.

22. Giera, W., V.M. Ramesh, A.N. Webber AN, I. van Stokkum I, R. van Grondelle, and K. Gibasiewicz. 2010. Effect of the P_{700} pre-oxidation and point mutations near A_0 on the reversibility of the primary charge separation in Photosystem I from Chlamydomonas reinhardtii. Biochim. Biophys. Acta. – Bioenergetics. 1797:106–112.

23. McConnell, M., J.B. Cowgill, P.L. Baker, F. Rappaport and K.E. Redding. 2011. Double reduction of plastoquinone to plastoquinol in photosystem 1, Biochemistry, 50:11034–11046.

24. Lefebvre-Legendre, L., F. Rappaport, G. Finazzi, M. Ceol, C. Grivet, G. Hopfgartner, and J.D. Rochaix. 2007. Loss of phylloquinone in Chlamydomonas affects plastoquinone pool size and photosystem II synthesis, J Biol Chem, 282: 13250-13263.

25. Hervás, M., J.A. Navarro, and M.A. De La Rosa. 2003. Electron transfer between membrane complexes and soluble proteins in photosynthesis. Acc. Chem. Res. 36:798 – 805.

26. Hope, A.B. 2000. Electron transfers amongst cytochrome f, plastocyanin and photosystem I: kinetics and mechanisms. Biochim. Biophys. Acta–Bioenergetics. 1456:5–26.